SHARPTON, Francis Arthur, 1936-
EXCITATION OF NEON ATOMS BY ELECTRON IMPACT.

The University of Oklahoma, Ph.D., 1968
Physics, spectroscopy

THE UNIVERSITY OF OKLAHOMA

GRADUATE COLLEGE

EXCITATION OF NEON ATOMS BY ELECTRON IMPACT

A DISSERTATION

SUBMITTED TO THE GRADUATE FACULTY

in partial fulfillment of the requirements for the

degree of

DOCTOR OF PHILOSOPHY

BY

FRANCIS ARTHUR SHARPTON

Norman, Oklahoma

1968

EXCITATION OF NEON ATOMS BY ELECTRON IMPACT

APPROVED BY

Robert M. St. John

William H. Huff

O. C. Simpson

E. E. Babb, Jr.

J. M. Campbell

DISSERTATION COMMITTEE

ABSTRACT

The cross sections of over 250 spectral lines of neon have been measured by the optical method. The estimated accuracy of the absolute experimental measurements was generally within a 20 percent limit, at least for the stronger lines. The approximate wavelength interval extends from 3300 to 12,000 Å. From the measured values determined for an incident electron energy of 100 eV of all 30 transitions belonging to the $2p \rightarrow 1s$ series, the apparent cross sections of the ten 2p levels have been obtained. Using experimental apparatus described in this report, the excitation functions of the ten 2p levels are plotted from onset to 200 eV.

The cross sections of the significant spectral lines belonging to the series $ns \rightarrow 2p$ and $nd \rightarrow 2p$ are tabulated. In those few cases where the cross sections could not be determined experimentally, the values are estimated by using theoretical transition probabilities. The final results yield the total cascade contribution into the 2p family for an incident electron energy of 100 eV. These show the cascade contribution to vary from eight percent for the $2p_1$ level to 67 percent for the $2p_{10}$ level. Comparisons are made between the experimental results and corresponding theoretical calculations obtained by employing the Born-Ochkur approximation.

The excitation functions of both the s and d levels are also presented. Similarities in these curves to those of helium are noted. Thus, the excitation functions of the pure triplet states are characterized by sharp peaks and fast declining tails, while those corresponding to levels connected to the ground state by optically allowed

transitions have very broad, nearly flat peaks.

An estimate was made of the contribution to the apparent cross sections of the 2s levels due to cascade from the 3p family. Theoretical transition probabilities were used to find the cross sections of the $3p \rightarrow 2s$ transitions from experimentally measured cross sections of spectral lines belonging to the $3p \rightarrow 1s$ family. The excitation cross sections of the 2s states which were determined in this manner are very sensitive to the inaccuracy of the wave functions employed to determine the transition probabilities. Therefore, the final results represent only qualitative estimates.

ACKNOWLEDGMENT

The author is indeed grateful to Dr. Robert M. St. John for his suggestion of this research problem and for his cooperation and support throughout the entire program.

My sincere appreciation is extended to Dr. C. C. Lin for his guidance and counsel on numerous occasions.

I would also like to convey my gratitude to Mr. Fred E. Fajen of the Los Alamos Scientific Laboratory, Los Alamos, New Mexico, for the theoretical data he supplied for this research, and Mr. James Hood and his staff in the Physics Shop for their cooperation and assistance in construction of the equipment.

To Jim Ballou, Paul Stanton and Jim Walker, for their assistance I wish to express my sincere thanks.

My family, Wanda and Jeffrey, have played an important role in this experience from its very inception and I will always be indebted for their constant encouragement. Wanda has patiently prepared the reading and final copies of this manuscript while Jeffrey found it impossible to understand why he could not help with the typing.

TABLE OF CONTENTS

LIST OF TABLES

LIST OF ILLUSTRATIONS

EXCITATION OF NEON ATOMS BY ELECTRON IMPACT

CHAPTER I

INTRODUCTION

The excitation of an atom by electron impact is a phenomenon of great practical interest. Most ion sources used in mass spectrometers and in apparatus for atomic collision studies are of the electron bombardment type. Collisional excitation and ionization are of great importance in astrophysics, upper atmospheric phenomena, thermonuclear research, plasma physics, and gaseous electronics. Experimental data on inelastic scattering are vital to the further development of the theory of atomic collisions for they provide tests of the assumptions and approximations that are necessarily made in theoretical calculations.

Accurate and detailed measurements of collision parameters have become possible only recently through advances in the technology of high gain photomultipliers and associated electronic amplification and noise rejection apparatus. The major contribution to the available excitation data has come from measurements and calculations on helium since it is the simplest monatomic atom. The study of the excitation of neon by electron impact provides useful comparisons to that of helium since both atoms are noble gases. As pointed out, however, by Anderson et al[1], experimental difficulties in using the optical method to determine

the direct excitation cross sections become more serious for the heavier atoms. The large number of spectral lines of the neutral atom makes it difficult to isolate the transitions which one wishes to study. This situation alone is probably the reason very little excitation cross section data for neon has been obtained.

The present work is by far the most comprehensive investigation of this subject. Relative and absolute measurements of the emission cross section of over 250 spectral lines in the approximate wavelength interval of 3300 to 12,000 Å are results of this experiment. Theoretical spontaneous transition probabilities have been employed where needed to facilitate calculation of the probability of excitation of a ground state neon atom experiencing an electron collision to a particular excited level. Such probabilities, or direct excitation cross sections as they are called, were calculated at an incident electron energy of 100 eV for the ten 2p levels. The resulting values obtained are compared to the theoretical calculations made by F. E. Fajen[2] using the Born and Born-Ochkur approximations. The branching ratios of spectral lines having common upper levels are calculated from the theoretical transition probabilities. Where possible these theoretical branching ratios are compared to those obtained by experiment, and conclusions are drawn from their agreement.

Theory

The passage of an electron through a gas will produce a number of different effects which result from the collision of the electron with the constituent atoms. These effects may be classified as being elastic, superelastic, or inelastic. In an elastic collision no energy is exchanged between the internal motion of the target atom and the colliding

electron. Superelastic collisions occur when the incident electron gains energy from the internal motion of the atom. When some of the kinetic energy of the colliding electron is lost in exciting the internal motion in the atom, the electron is said to have experienced an inelastic collision. Further division of the latter case involves knowing whether the collision produces single excitation, double excitation, ionization, or ionization-excitation. This work deals exclusively with the process of single excitation.

In order to represent quantitatively the probability that an electron with sufficient energy will produce excitation of a ground state atom as a result of the collision, the concept of cross section is employed. The equation expressing the cross section in terms of experimentally measurable quantities may be obtained from a consideration of the production rate of excited species. Thus, letting N_j be the number of excited atoms produced per cubic centimeter by the electron beam, the population equation under the assumption of single neutral atom-electron collisions becomes

$$\frac{dN_j}{dt} = NQ_j n_e + \sum_{i>j} A_{ij} N_i - N_j \sum_{k<j} A_{jk} \quad . \qquad (1)$$

In this equation n_e is the number of electrons passing through the gas per second per square centimeter of the beam, Q_j is the cross section for excitation to the jth level, N is the number of ground state atoms per cubic centimeter, and A_{ij} is the probability per second that an excited atomic electron will make a transition from the ith to the jth level. The A_{ij}'s are technically called the spontaneous Einstein transition probabilities. Under steady state conditions, i.e. when N_j is a

constant, equation (1) becomes

$$NQ_j n_e = N_j \sum_{k<j} A_{jk} - \sum_{i>j} A_{ij} N_i \quad . \tag{2}$$

The direct excitation cross section Q_j can, therefore, be expressed in terms of the cascading contributions to and from the jth level.

The total number of photons emitted per centimeter of the electron beam, with frequency corresponding to the $j \rightarrow k$ transition, is given by

$$J_{jk} = A_{jk} \int_S N_j \, dS \quad , \tag{3}$$

where S is the cross sectional area of the beam.

The electron beam current is given by

$$I_e = e \int_S n_e \, dS \quad , \tag{4}$$

where e is the electronic charge.

In order to obtain the total number of excited atoms produced per centimeter of electron beam, it is necessary to multiply equation (2) on both sides by dS and integrate the resulting expression over the total area of the beam. When this has been done and equations (3) and (4) have been substituted, the following result is obtained:

$$NQ_j \left(\frac{I_e}{e}\right) = \frac{J_{jk}}{A_{jk}} \sum_{k<j} A_{jk} - \sum_{i>j} J_{ij} \quad . \tag{5}$$

This expression takes on a simpler form by introducing the so-called theoretical branching ratio, B_{jk}. This quantity is defined as the ratio of the total transition probability, for radiative transitions from the jth level to all lower levels, to the transition probability of a radiative transition from the jth to the kth level. When B_{jk} is substituted

into equation (5), the direct excitation cross section to the jth level becomes

$$Q_j = B_{jk} \frac{J_{jk}}{N\left(\frac{I_e}{e}\right)} - \frac{\sum_{i>j} J_{ij}}{N\left(\frac{I_e}{e}\right)} \quad . \tag{6}$$

Defining the cross section of the spectral line in question by the expression

$$Q_{jk} = \frac{J_{jk}}{N\left(\frac{I_e}{e}\right)} \quad , \tag{7}$$

equation (6) becomes

$$Q_j = B_{jk} Q_{jk} - \sum_{i>j} Q_{ij} \quad . \tag{8}$$

Thus, the direct excitation cross section depends upon three quantities which correspond to different steps of the analysis. The initial experimental measurements yield cross sections of radiative transitions which depend upon the absolute intensities of the emitted spectral lines for a given electron beam current and number density of ground state atoms. These are converted into apparent excitation cross sections by multiplying each by its respective theoretical branching ratio. Subtracting the cascade contributions from the apparent excitation cross section yields the direct excitation cross section. This latter quantity, which might be thought of as describing the effectiveness of populating an excited level by collisions of electrons with ground state atoms, is of prime importance. The efforts of this work have been directed to the evaluation of this quantity for the ten 2p excited states of neon.

CHAPTER II

EXPERIMENTAL APPARATUS

The experimental apparatus which is used to measure excitation cross sections by the optical method may be divided into four constituent components:

(1) a vacuum system modified to permit introduction of the neon atoms into the collision region,

(2) an electron gun to produce the incident particles and to control their energy,

(3) light detection and data processing equipment to convert the photon radiation into useful information, and

(4) an absolute photon standard to calibrate the detection system. This chapter will describe the more important aspects of the first three of these components used in this study and the following chapter will deal exclusively with the fourth component.

The Vacuum System

The vacuum system, with the exception of a glass McLeod gauge and the gas reservoir, is made exclusively of metal. The principal building material is stainless steel. Glass to metal seals were installed to join the glass and metal portions. The system was designed so that it could be disassembled for cleaning whenever the need might arise. The various sections of the system are coupled together by Conflat flanges

manufactured by Varian Associates. The main vacuum chamber which houses the electron gun was designed to permit baking at temperatures up to 400°C. After the initial roughing of the system by either a mechanical or a cryogenic forepump to pressures of 5×10^{-4} Torr, the foreline is valved off and the main vacuum chamber is then opened to a Varian VacIon pump. The pressure in this part of the system after sufficient baking will reach an ultimate pressure of 3×10^{-9} Torr. Thus, impurities from the residual gases are negligible since the actual experiment is performed with neon gas pressures in the micron range.

The number density of the neon atoms is determined by measuring the pressure in the collision chamber by employing a McLeod gauge connected by an appendage through a cold trap to the chamber. When not in use or when the trap is not cooled, the McLeod gauge is valved off from the rest of the system in order to keep mercury vapors from getting into the collision region. During these times a Pirani gauge calibrated relative to the McLeod is employed to monitor the gas pressure.

The neon gas was purchased from the Linde Corporation in liter glass flasks containing the gas at a pressure of one atmosphere. Dosing the system from the Linde bottle is facilitated by employing two metal valves in series with each other and having a small volume between them. Thus, opening the valve next to the bottle fills the small volume with gas. Closing this valve and opening the second introduces the metered amount of gas into the system.

A photograph of the vacuum system showing the collision chamber and the McLeod gauge is shown in Figure 1. Also shown in this figure are the monochromator and associated optics, since the vacuum system and the

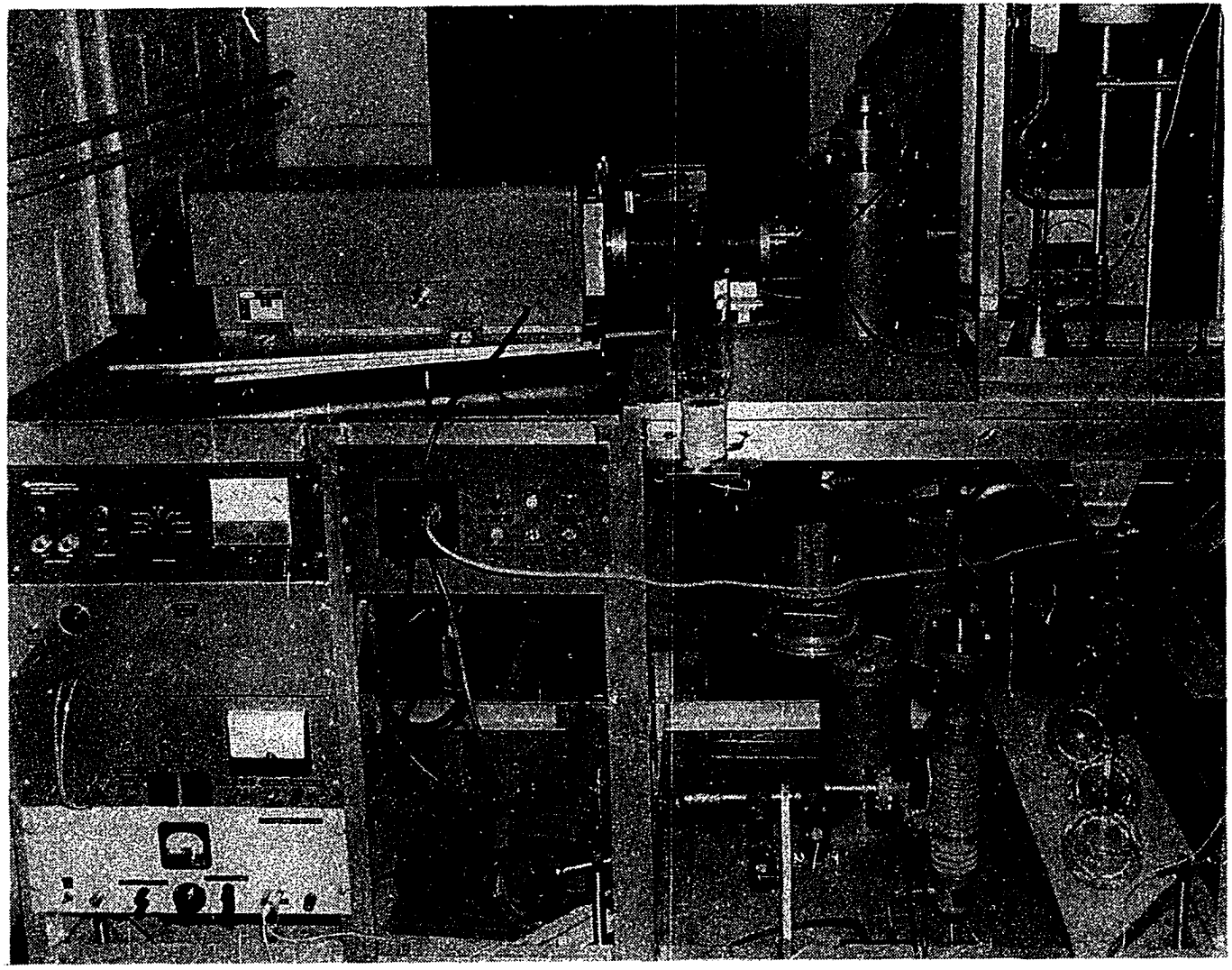

FIGURE 1. Experimental Apparatus

monochromator are situated on the same table which is built of aluminum.

The Electron Gun

The neon atoms are excited by a well collimated beam of nearly monoenergetic electrons. The beam is produced by an electron gun which is built of stainless steel. Insulation of the various electrodes is accomplished by employing glass beads two millimeters in diameter. The gun, displayed in Figures 2 and 3, is of pentode design. An indirectly heated barium impregnated cathode provides the electron source. The electrons emitted from the cathode are accelerated and collimated by focusing grids which act as pinhole lenses to the electrons. The resulting collimated beam which is approximately two millimeters in diameter passes into a cylindrical Faraday cage or a field-free region where they are collected by the walls of the cage, and the resulting beam current is measured with an accurate microammeter. The radiation resulting from the excitation is observed at right angles to the electron beam through a small window in the side of the Faraday cage. In order to minimize back scattering of the beam and the effects of secondary electrons which might get into the interaction region, an electron collector operated at a positive voltage with respect to the Faraday cage was installed just behind the metal screen which acts as the rear wall of the field-free region.

The maximum output beam current from this particular electron gun may reach values of only 2.5 milliamperes. The actual maximum current attainable will depend, of course, upon the pressure of the particular gas which is being studied and the temperature of the cathode. For the studies in neon, electron beam currents were always 500 microamperes or less. Currents of 50 microamperes were very common.

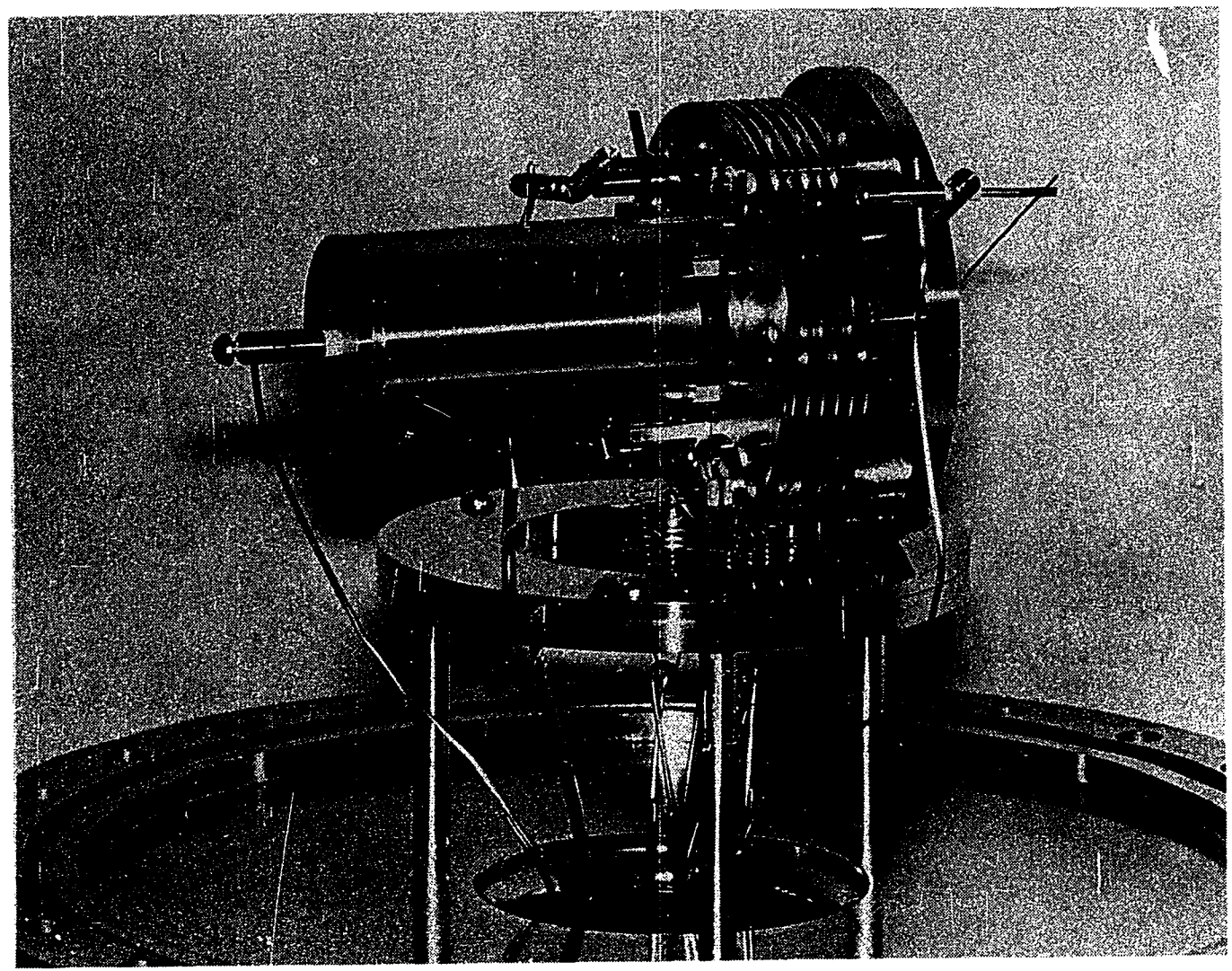

FIGURE 2. Electron Gun

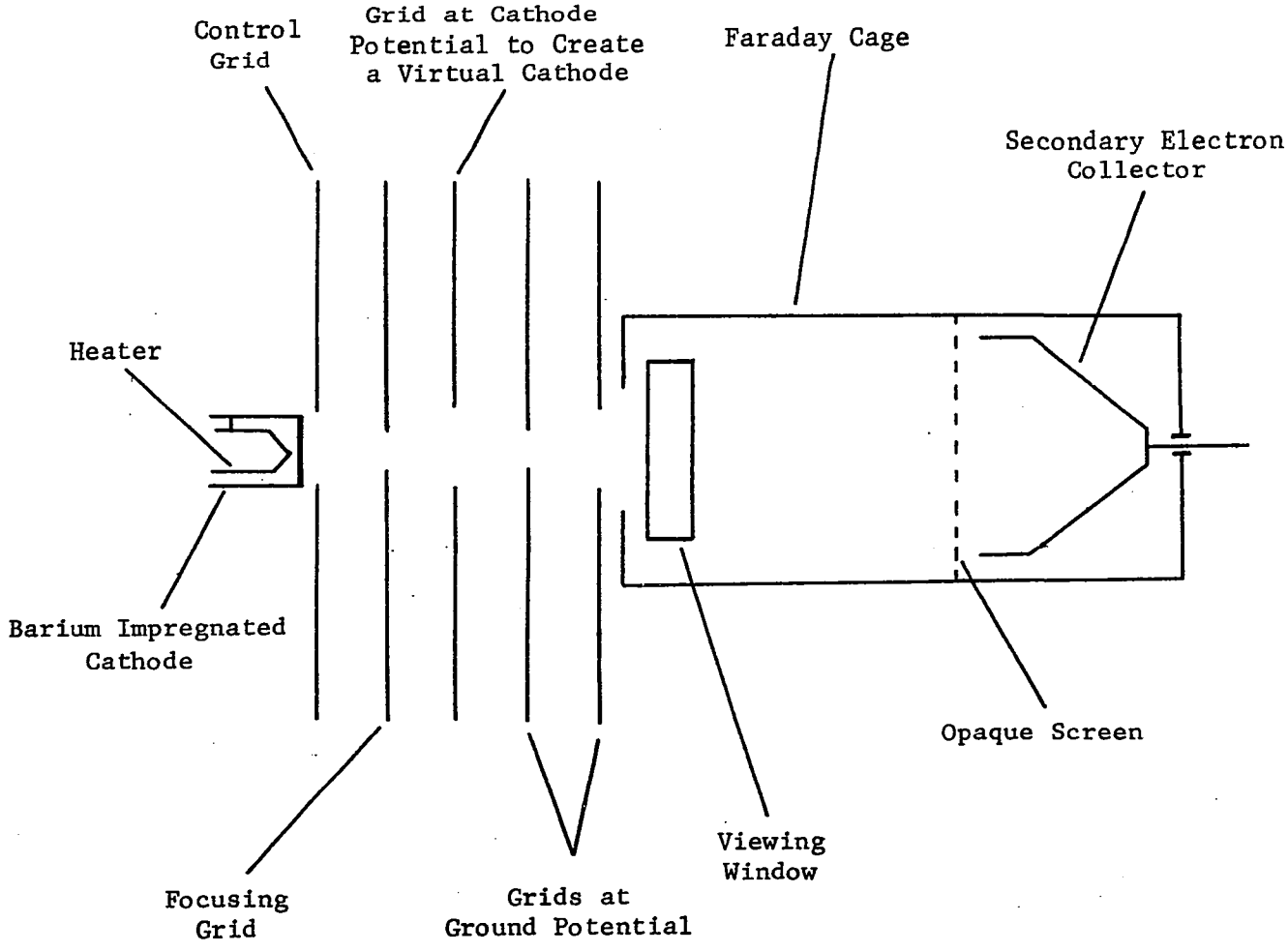

FIGURE 3. Electron Gun Schematic

In the neon studies the incident electrons always had an energy distribution which was less than 1 eV. This upper limit may be placed upon the distribution in the energy of the incident electrons through an examination of the fine structure found in the excitation function of the $2p_{10}$ level of neon. The 1 eV upper limit placed on this particular electron gun is not too surprising since other guns of this design have been shown by retarding potential measurements to have energy resolution in the vicinity of 0.5 eV.

The Light Detection and Automatic Data Processing Equipment

From equation (7) it can be seen that the cross section Q_{jk} of a spectral line can be obtained as a function of energy by varying the energy of the incident electrons and measuring the light output J_{jk} while at the same time the number density N and the electron beam current I_e are held constant. A plot of this type is called an excitation function.

The electronic equipment employed to automatically perform these tasks is displayed along with other related experimental apparatus in a block diagram in Figure 4. A programmed regulated D.C. power supply continuously changes the energy of the incident electrons.

The Constant Current Device

The electron beam flux is held constant over the range from 18 to 200 eV by a degenerative feedback system described by Anderson et al[1]. In this system the electron beam current into the interaction region is sampled by monitoring the voltage produced across a resistor which has been placed in the return path from the Faraday cage-collector system. When the electron beam current exceeds a pre-determined level, a current

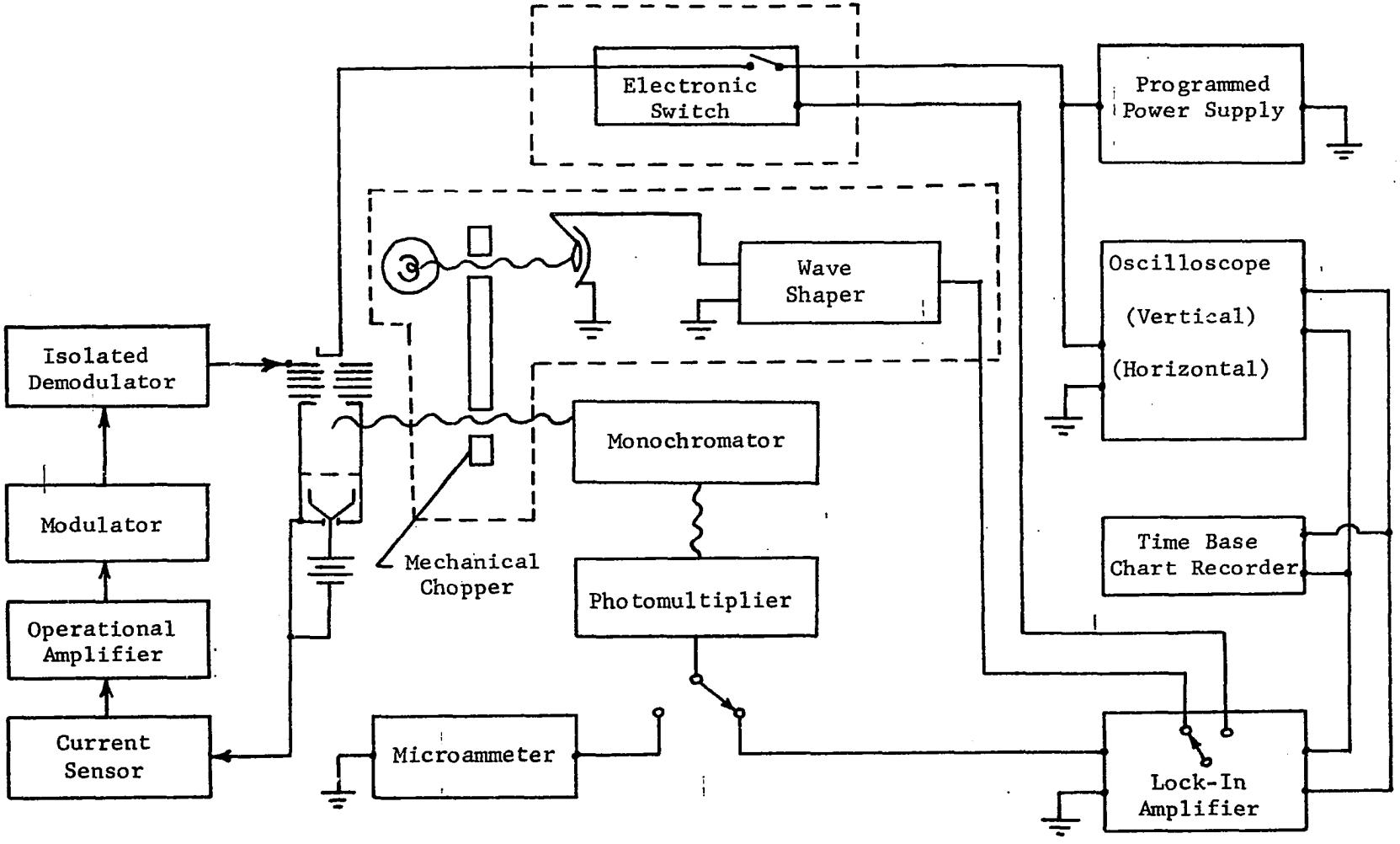

FIGURE 4. Light Detection and Data Processing System

(Only one modulation system is used at a time.)

comparator converts the difference between the value of the actual and that of the desired current into a voltage signal. This signal is amplified by an operational amplifier which is essentially a chopper stabilized D.C. amplifier that is operated with negative feedback so that greater stability will be obtained. Since the cathode of the electron gun must be operated at a negative potential, with respect to the Faraday cage, it is necessary to isolate this control signal before it is applied to the first grid of the electron gun where the focusing characteristics are adjusted and, hence, the electron beam current regulated. In order for isolation to be accomplished the control signal is used to modulate a 50 KHz carrier wave. After amplification, the modulated signal is then demodulated, filtered to remove unwanted carrier signal, and then applied to the first grid of the electron gun. A detailed circuit diagram of the constant current control unit, along with some relevant statistics pertaining to its stability, is given by Anderson[3].

In some cases larger currents were required from the gun than those which could be satisfactorily regulated by the constant current controller. For these exceptions the pentode characteristic nature of the gun was utilized. Thus, it was found that the current could be regulated manually quite satisfactorily from onset to energies up to approximately 60 eV. From this energy up to 400 eV only slight periodic adjustment of the second grid will hold the current constant. Hence, excitation functions can be plotted with this semi-automatic method.

The Optical System

The radiation produced as a result of the excitation processes is observed perpendicular to the beam direction. The light contained within

the solid angle subtended by an aperture stop which immediately precedes a lens is focused by the latter upon the entrance slit of a half-meter Ebert mounted Jarrell-Ash grating monochromator. The grating angle may be varied either manually or by an electric scanning motor. With this instrument a range of wavelengths from 2000 to 18,000 Å may be covered by interchanging two gratings. Thus, the desired spectral transition may be selected and the resulting light passing through the exit slit will be detected by a high gain photomultiplier tube.

Further discussion of the optical system is given in Chapter III.

Photomultiplier Tubes

Four distinct photomultiplier tubes are used as the need arises. The choice of detector depends upon its spectral response, gain, dark current, and cathode sensitivity. For the visible region from 3000 to 6000 Å an EMI 6256A photomultiplier is used. This tube has a S-13 spectral response. In the spectral region from 6000 to 8000 Å either an EMI 9558A or a RCA 7265 tube is employed. These tubes possess a S-20 spectral response. For the near infrared from 8000 to 12,000 Å a RCA 7102 with a S-1 spectral response is chosen. The dynode voltages of the photomultiplier tube are supplied by a Model RE-3002 high voltage power supply built by the Northeast Scientific Corporation. The signal from the photomultiplier is measured in the D.C. mode by reading the output with a Model 610B Keithley electrometer and microammeter. Dark current caused by thermal electron emission from the cathode is reduced when the need arises by cooling to liquid nitrogen temperature the photomultiplier tube in a specially built cryostat which is attached to the monochromator.

Modulation Techniques

Excitation cross sections are, in general, measured under conditions

of low electron beam current densities and target gas number densities. This situation produces photomultiplier signals which in most cases are only slightly larger than the dark current or noise of the detector. Thus, in order to enhance the signal to noise ratio, in addition to cooling the photomultiplier, A.C. modulation techniques have been adopted. In order to achieve this purpose two distinct forms of modulation have been devised. The most frequently used method is to chop the light coming from the interaction region with a rotating wheel containing equally spaced circular holes located near the wheel's edge. The holes in the wheel are positioned so that equal intervals of light passage and light blockage occur. Thus, a square modulated light signal of 1 KHz is fed to the input of a tuned amplifier and phase detector. The phase detector requires that a reference signal of the same frequency as the chopped light be fed to a diode bridge network contained within its circuitry. This reference signal is obtained from a photocell which detects the light from a small bulb placed diametrically opposite the aperture through which the radiation from the collision region passes. The output of the photocell is then passed into a wave shaping circuit to provide a sine wave reference to the phase detector.

The second method of modulating the radiation from the collision region consists in switching the electron beam on and off by an electronic switch. When this form of modulation is desired the reference light circuitry is disconnected from the phase detector and the chopper wheel is removed from the front of the monochromator entrance slit. The electronic chopper is then placed in the line running from the programmed D.C. power supply to the accelerating grid of the electron gun. The phase detector is now switched to an internal mode where it will supply

its own reference as well as a signal at the same frequency to drive the electronic chopper.

Scanning through the same portion of the visible spectrum using either mode and recording the separate results with a strip chart recorder reveals that the signal to noise ratio of the photomultiplier output is about equal for both modulation techniques. However, for radiation having wavelengths greater than about 7500 Å, i.e. when the photomultiplier tube having a S-1 spectral response must be used, it is necessary to adopt the latter method and, hence, chop the beam rather than the light so that the background radiation will not be modulated.

The Lock-In Amplifier

The modulated signal from the photomultiplier is fed into a Princeton Applied Research Lock-In Amplifier Model JB-4. The PAR Lock-In amplifier consists essentially of four sections. The input signal first enters a tunable amplifier, the desired frequency being externally selected by turning a dial on the front panel of the device. The tuned amplifier output is next fed into a phase sensitive detector which selectively rectifies the A.C. signal by comparing it with a reference signal of the same frequency in a diode bridge network. The reference signal comes from the reference generating section of this instrument. Maximum sensitivity of this device is obtained by adjusting the two signals so that they are in phase with each other after being rectified by the diode bridge network. After detection the resulting signal then goes to the D.C. section where it is integrated in a RC network and amplified in a D.C. amplifier. The tuned amplifier of the Model JB-4 has a Q of about 25 and it further reduces the amplitude of any component of the incoming signal which is not at the modulation frequency.

This instrument can either generate its own reference signal and at the same time provide an output to drive a modulating device such as the electronic chopper, or it can be adjusted so that it will accept an externally generated reference such as the one from the mechanical chopper. The PAR Lock-In amplifier can handle frequencies ranging from 15 Hz to 15 KHz. It has an equivalent bandwidth of 0.024 Hz when maximum RC integrating time is used. This unit is capable of recovering a signal which is 46 db below the ambient white noise in a 1 KHz band centered about the signal frequency with a signal to noise ratio of one.

The Oscilloscope

The excitation functions are plotted by feeding the D.C. output of the Lock-In amplifier to the vertical deflection plates while the electron energy supplied by the programmed D.C. power supply is impressed upon the horizontal input of a Tektronix Model 561A oscilloscope. A Model C-12 Tektronix camera with an attached Model 100 projected graticule to eliminate parallax and a Polaroid film holder set for time exposure makes a permanent record of the beam dot as it traces out the excitation function on the oscilloscope screen. The resulting photograph yields a relative measurement of Q_{jk} versus electron energy in the form of a continuous plot.

The Chart Recorder

When it is desired to measure the absolute cross sections of several atomic transitions in an element such as neon the oscilloscope is replaced by a Model V.O.M. 7 Bausch and Lomb strip chart (time base) recorder. Thus, holding the number density and the electron beam current constant while the spectrum of interest is scanned by the monochromator at a given electron energy, the output from the Lock-In amplifier, which

is now fed into the chart recorder, will yield recorder deflections which are proportional to the cross sections of the respective atomic lines. Scanning the same region of the spectrum when the radiation is emitted from a tungsten ribbon lamp which has been calibrated so that absolute photon rates may be obtained will yield deflections on the chart recorder which may be used to calibrate those produced when the radiation was emitted from the collision region. A discussion of the standardization theory is deferred to the following chapter.

CHAPTER III

STANDARDIZATION OF THE DETECTION SYSTEM

From equation (7) it is shown that the cross section of a particular radiative transition is given by

$$Q_{jk} = \frac{J_{jk}}{N\left(\frac{I_e}{e}\right)} \quad , \tag{7}$$

where J_{jk} is the total number of photons emitted per second per centimeter of the electron beam for the frequency corresponding to the $j \rightarrow k$ transition. Thus, Q_{jk} depends upon an accurate measurement of the absolute intensity of the emitted spectral line. Through consideration of the optical system and by making direct comparisons of the photomultiplier signals from the beam with those from a calibrated tungsten ribbon source, absolute intensity measurements are obtained.

The radiation produced as a result of the collision process is observed at an angle of 90° with respect to the electron beam. The light emitted from the interaction region into a known solid angle Ω_{cc} subtended by the collision chamber lens stop is imaged with unit magnification upon the entrance slit of a monochromator. The selected wavelength of light which emerges from the exit slit of this instrument diverges sufficiently to permit illumination of a large area of the cathode surface of a high gain photomultiplier tube which is placed

directly in front of the slit. This selected geometry eliminates inaccuracies due to sensitivity variations over the cathode surface. The output current, I_{cc}, from the photomultiplier tube is dependent not only on J_{jk} and Ω_{cc} but also upon the effective length, Δx, of the beam from which radiation is observed, the transmission properties, $T_{cc}(\lambda)$, of the optical system, and the photon efficiency, $E(\lambda)$, of the detector. The equation relating these quantities is given by

$$I_{cc} = J_{jk} \left(\frac{\Omega_{cc}}{4\pi}\right) \Delta x \; T_{cc}(\lambda) \; E(\lambda) \quad , \tag{9}$$

where the factor 4π is the total solid angle through which photons are radiated.

The wavelength dependence of $E(\lambda)$ is determined by measuring the output current, I_{SL}, from the photomultiplier tube when the radiation is emitted from a tungsten ribbon lamp, which replaces the collision chamber as the photon source. This lamp, Model Number T24/2, was manufactured by the General Electric Company with calibration measurements traceable to the National Bureau of Standards.

Defining $J_{SL}(\lambda,T)$ as the number of photons emitted by the tungsten surface at a temperature T per second, per wavelength interval, per square centimeter of ribbon area, per unit solid angle subtended by the same, the equation expressing I_{SL} in terms of experimentally measurable quantities and $E(\lambda)$ may be written as

$$I_{SL} = \Omega_{SL} \; A_{SL} \int_{\lambda_1}^{\lambda_2} E(\lambda) \; J_{SL}(\lambda,T) \; T_{SL}(\lambda) \; d\lambda \quad . \tag{10}$$

In this equation Ω_{SL} and $T_{SL}(\lambda)$ have the same relationship to the standard lamp as Ω_{cc} and T_{cc} have to the collision chamber, and A_{SL} is the effective area of the standard lamp from which radiation is detected.

The integral in equation (10) must be evaluated over the transmitted wavelength band of the monochromator.

Assuming $E(\lambda)$ to be equal to $E(\lambda_o)$, where λ_o is the wavelength of the radiation corresponding to the $j \rightarrow k$ transition, equations (9) and (10) may be combined to obtain J_{jk}. The result is

$$J_{jk} = 4\pi \frac{I_{cc}}{I_{SL}} \left(\frac{\Omega_{SL}}{\Omega_{cc}} \frac{A_{SL}}{\Delta x}\right) \frac{\int_{\lambda_1}^{\lambda_2} J_{SL}(\lambda, T)\, T_{SL}(\lambda)\, d\lambda}{T_{cc}(\lambda)} \quad . \tag{11}$$

The quantity $J_{SL}(\lambda, T)$ is obtained from Planck's radiation law through black body considerations. In the following section the necessary equation is derived.

Black Body Theory

Planck's radiation law for the equilibrium distribution of energy from an ideal black body is

$$U_\lambda^B = \frac{8\pi\, hc}{\lambda^5 \left[e^{hc/\lambda kT} - 1\right]} \quad . \tag{12}$$

U_λ^B may be called the "monochromatic energy density" of black body radiation. It has units of energy per unit volume per unit wavelength interval. Thus, $U_\lambda^B\, d\lambda$, which has units of energy density, is the amount of energy contained in unit volume in the form of black body radiation in a wavelength range $d\lambda$ at wavelength λ.

Black body radiation may be treated mathematically by considering the radiant energy contained within the interior of a hollow heated cavity. Since cavity radiation is completely independent of the size or shape of the cavity, being dependent only on the temperature, no loss of generality results if the cavity is assumed to be the interior of a sphere of very large radius.

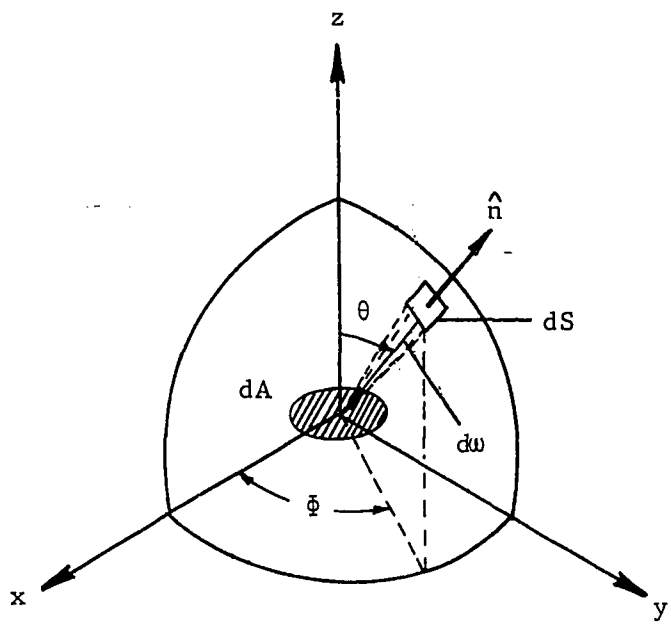

FIGURE 5. Geometrical Representation of Black Body Radiation

Referring to Figure 5, let dA be a small surface element of a radiating body located at the center of the spherical cavity and perpendicular to the z-axis. Also, let dS designate a small element of area on the surface of the sphere. Then it is easily seen that the radiated power dR_p from the surface dA and incident upon dS will be proportional to the area dA and the element of solid angle dω of which the area dS subtends at the origin of coordinates. It will also depend upon the angle θ between the directed areas $\vec{dA}$ and $\vec{dS}$. Therefore,

$$dR_p = I^B dA \cos\theta \, d\omega \quad , \tag{13}$$

where I^B is called the total intensity of radiation per unit solid angle from the element of radiating surface and along its normal. $I^B \cos\theta$

represents the rate at which radiant energy is emitted in the direction n per unit solid angle and per unit of its own area. In a cavity I^B from the walls takes on the value for a truly black body radiator since what the walls fail to radiate is made up for by reflection.

Now all rays drawn from points on dA to points on dS may be considered parallel since the sphere has such large radius and also dS may be chosen of such size that it is the exact projection of dA in the direction of n. The radiant energy emitted in one second from dA in the direction of n will be contained, therefore, in a cylinder of length c (the speed of light which is assumed to be in a vacuum) and area dA cos θ. Therefore, the volume of this cylinder is

$$dV = c\ dA \cos\theta \quad . \tag{14}$$

The magnitude of the radiant energy in the cavity is just simply dR_p times one second. Therefore, multiplying equation (13) by one second and dividing the result by dV, the energy density due to this radiation anywhere inside the cylinder is

$$d\left[U_\lambda^B\ d\lambda\right] = \frac{I^B}{c}\ d\omega \quad . \tag{15}$$

Assuming I^B to be uniform in all directions, this last expression can be integrated over the entire sphere. The result obtained is

$$U_\lambda^B\ d\lambda = \frac{I^B}{c} \int_0^{2\pi} \int_0^{\pi} \sin\theta\ d\theta d\Phi = \frac{4\pi}{c}\ I^B \quad . \tag{16}$$

Therefore,

$$I^B = \frac{c}{4\pi}\ U_\lambda^B\ d\lambda \quad . \tag{17}$$

Non-Black Body Modifications

Since the radiating surface of the standard lamp is made of tungsten, I^B of equation (17) must be modified by multiplying it by the emissivity

$e(\lambda,T)$ of this material. Hence,

$$I = e(\lambda,T)\ I^B = \frac{c}{4\pi}\, e(\lambda,T)\ U_\lambda^B\, d\lambda \quad . \tag{18}$$

Equation (18) may be modified to find the rate of emission of photons per unit wavelength interval from a unit area of the tungsten ribbon into a unit solid angle normal to its surface. This quantity designated by $J_{SL}(\lambda,T)$ is given by

$$J_{SL}(\lambda,T)d\lambda = \frac{I}{h\nu} = \frac{c}{4\pi h\nu}\, e(\lambda,T)\ U_\lambda^B\, d\lambda \quad , \tag{19}$$

where h is Planck's constant and ν is the frequency of the light emitted from the standard lamp. Therefore, since $\nu = \frac{c}{\lambda}$, $J_{SL}(\lambda,T)$ is given by

$$J_{SL}(\lambda,T) = \frac{c}{4\pi h}\, e(\lambda,T)\ U_\lambda^B \quad . \tag{20}$$

Transmission Characteristics of the Monochromator

In order to determine the number of photons which get out of the monochromator exit slit, it is necessary to know the transmission characteristics of the monochromator. According to Harrison and Lord[4] the relative transmission of a grating monochromator having its entrance and exit slit widths equal will have the triangular pattern shown in Figure 6.

From Figure 6

$$T_{Rel}(\lambda) = \begin{cases} 1 + \frac{\lambda}{\Delta\lambda} \ , & -\Delta\lambda \le \lambda \le 0 \\ 1 - \frac{\lambda}{\Delta\lambda} \ , & 0 \le \lambda \le \Delta\lambda \end{cases} \tag{21}$$

If W is the width of the slits, f the focal length of the monochromator, and $\frac{d\theta}{d\lambda}$ the dispersion of the instrument, then $\Delta\lambda$ is

$$\Delta\lambda = \frac{W}{f\,\frac{d\theta}{d\lambda}} \quad . \tag{22}$$

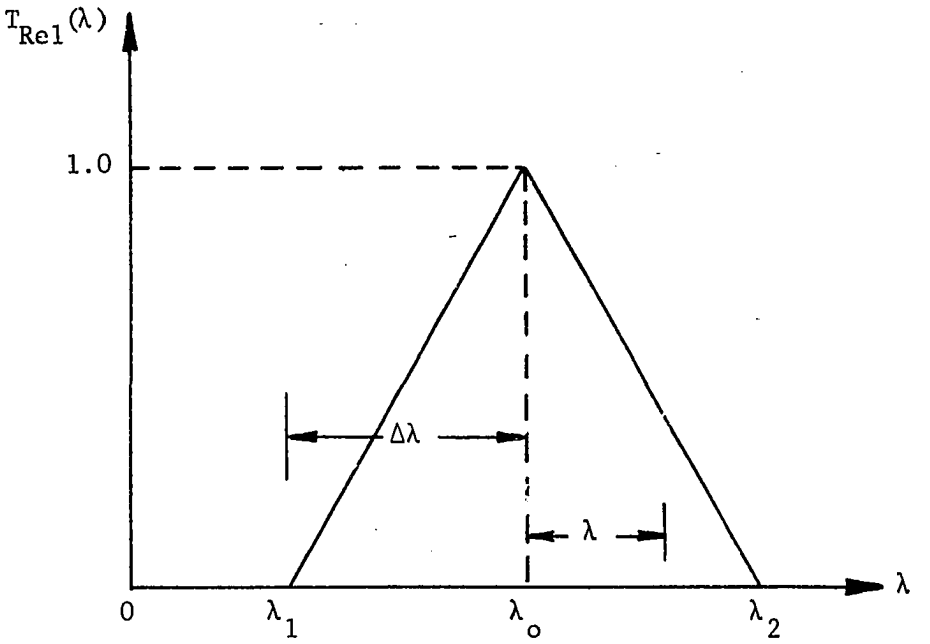

FIGURE 6. Relative Transmission of a Grating Monochromator With Equal Entrance and Exit Slit Widths

A Jarrell-Ash one-half meter scanning monochromator fitted with a grating having 1180 grooves per millimeter gives a value for $\Delta\lambda$ of approximately 16 $\mathring{A}$ when the slit jaws are set for a one-millimeter separation.

Returning now to the evaluation of the quantity

$$\frac{1}{T_{cc}(\lambda)} \int_{\lambda_1}^{\lambda_2} J_{SL}(\lambda, T)\ T_{SL}(\lambda)\ d\lambda$$

in equation (11), it is necessary to ascertain that $\frac{T_{SL}(\lambda)}{T_{cc}(\lambda)}$ is merely $T_{Rel}(\overline{\lambda})$. In order to make the optical path from the standard lamp simulate that from the collision chamber, it was decided to mount the standard lamp, imaging lens, monochromator, and photomultiplier tube

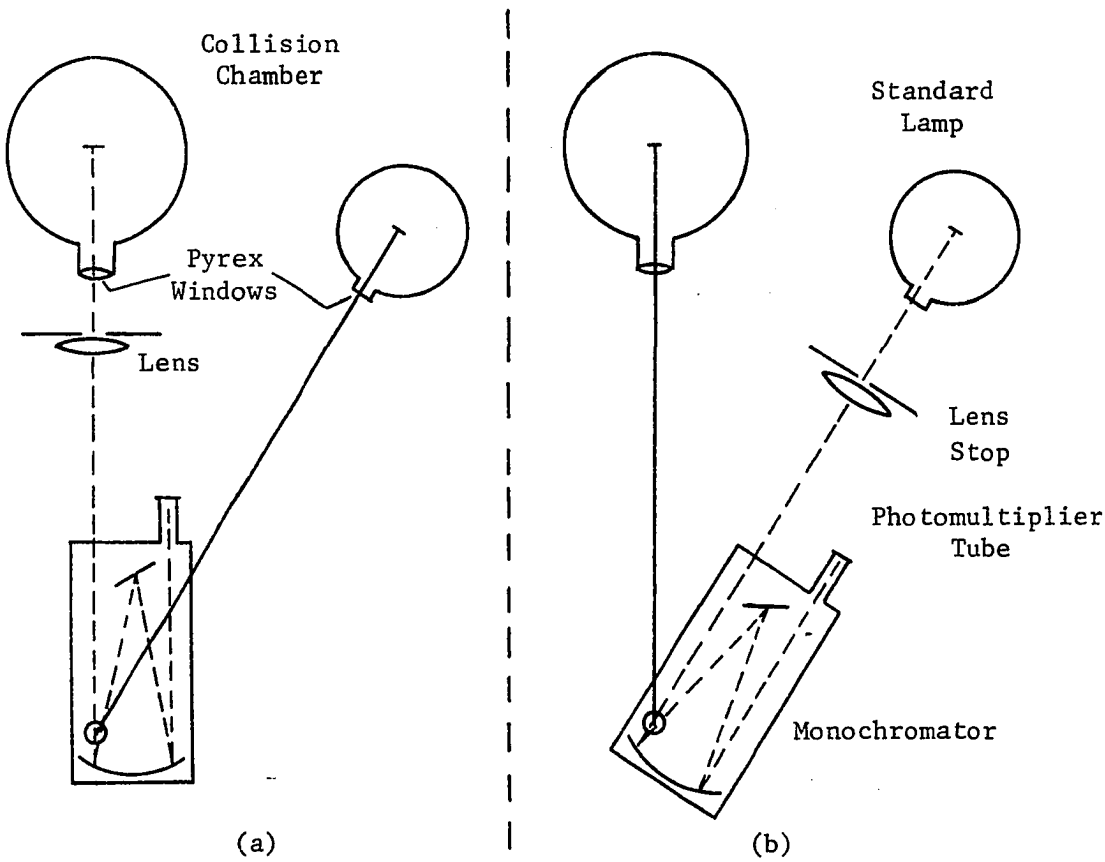

FIGURE 7. Optical Arrangement for Standardization

(a) Collision chamber as light source
(b) Standard lamp as light source

so that the latter three could be rotated as a unit to admit radiation from either the collision chamber or the standard lamp. The experimental arrangement is shown above in Figure 7. Since both viewing windows are made of pyrex and the lens, image and object distances are the same for both modes, this arrangement is equivalent to replacing the collision chamber by the standard lamp.

Referring again to the triangular wavelength band pass of Figure 6 which results from the standard lamp light and to the experimental

arrangement of Figure 7, it follows that $T_{SL}(\lambda) = KT_{Rel}(\lambda)$ where K has a value less than unity. Also, since the light from the collision chamber has the wavelength λ_o, it follows that the transmission function $T_{cc}(\lambda)$ will depend only on K. Hence,

$$\frac{T_{SL}(\lambda)}{T_{cc}(\lambda_o)} = T_{Rel}(\lambda) \quad . \tag{23}$$

The factor

$$\int_{\lambda_1}^{\lambda_2} J_{SL}(\lambda,T) \frac{T_{SL}(\lambda)}{T_{cc}(\lambda_o)} d\lambda = \int_{\lambda_1}^{\lambda_2} J_{SL}(\lambda,T)\ T_{Rel}(\lambda)\ d\lambda \tag{24}$$

may now be evaluated. From equations (12), (20), and (21), equation (24) becomes

$$\int_{\lambda_1}^{\lambda_2} J_{SL}(\lambda,T)\ T_{Rel}(\lambda)\ d\lambda = \int_{-\Delta\lambda}^{o} \frac{2c\ e(\lambda,T)}{\lambda^4\left[e^{hc/\lambda kT} - 1\right]}\left(1 + \frac{\lambda}{\Delta\lambda}\right) d\lambda$$

$$+ \int_{o}^{\Delta\lambda} \frac{2c\ e(\lambda,T)}{\lambda^4\left[e^{hc/\lambda kT} - 1\right]}\left(1 - \frac{\lambda}{\Delta\lambda}\right) d\lambda \quad . \tag{25}$$

Obviously, an exact evaluation of these two integrals would be impossible. However, an examination of the functions $e(\lambda,T)$ and

$$J^B_{SL}(\lambda,T) = \frac{2c}{\lambda^4\left[e^{hc/\lambda kT} - 1\right]}$$

over the interval of interest reveals that the emissivity of tungsten may be assumed constant and J^B_{SL} may be considered to vary linearly with wavelength, i.e.

$$J^B_{SL}(\lambda,T) = J^B_{SL}(\lambda_o,T) + S\lambda \quad , \tag{26}$$

where

$$S = \frac{\Delta \left[J^{B}_{SL}(\lambda, T) \right]}{\Delta \lambda}$$

is the slope of the curve which is very nearly a constant over the interval. These approximations are indeed quite accurate for values of $\Delta\lambda \leq 20$ Å in the visible region of the spectrum and are even accurate for values of $\Delta\lambda \leq 200$ Å in the infrared.

When these approximations are substituted into equation (25) and the two integrals are then evaluated, the final result is

$$\int_{\lambda_1}^{\lambda_2} J_{SL}(\lambda, T)\ T_{Rel}(\lambda)\ d\lambda = \frac{2c\ e(\lambda_o, T)\ \Delta\lambda}{\lambda_o^4 \left[e^{hc/\lambda_o kT} - 1 \right]} \quad . \qquad (27)$$

This result shows that the number of photons passing out of the exit slit of the monochromator per second per unit area of the tungsten ribbon per unit solid angle subtended by the aperture stop is obtained by multiplying $J_{SL}(\lambda, T)$ by $\Delta\lambda$, which is the width of the curve at half the maximum height of the transmission function.

In actual practice, especially when $W \leq 0.25$ millimeter, it has been found that the transmission function, $T_{Rel}(\lambda)$, does not have the triangular form as shown in Figure 6, but it has a form which is more closely approximated by a trapezoidal function. This, however, adds no additional complication to the evaluation of the integrals in equation (25). The result in this case is exactly the same and $\Delta\lambda$ still means the width of the curve at half the maximum height of the measured transmission function.

If the result obtained in equation (27) is substituted into equation (11), J_{jk} becomes

$$J_{jk} = 4\pi \frac{I_{cc}}{I_{SL}} \left(\frac{\Omega_{SL} A_{SL}}{\Omega_{cc} \Delta x}\right) P_{\Delta\lambda} \quad , \tag{28}$$

where

$$P_{\Delta\lambda} = \frac{2c\, e(\lambda_o, T)\, \Delta\lambda}{\lambda_o^4 \left(e^{hc/\lambda_o kT} - 1\right)} \quad . \tag{29}$$

Values of $P_{\Delta\lambda}$ for a range of temperatures and wavelengths have been calculated by employing the emissivities reported by deVos[5] for a bandwidth, $\Delta\lambda = 16$ Å, with an IBM 1040 electronic computer.

When equation (28) is substituted into equation (15), the cross section of the $j \rightarrow k$ transition becomes

$$Q_{jk} = 4\pi \left(\frac{I_{cc}}{I_e I_{SL}}\right) \frac{P_{\Delta\lambda}}{(N/e)} \left(\frac{\Omega_{SL} A_{SL}}{\Omega_{cc} \Delta x}\right) \quad . \tag{30}$$

From equation (30) absolute cross sections may be obtained. It is only necessary to determine the unknown parameters. The currents I_{cc}, I_{SL}, and I_e are determined from accurately calibrated current instruments. The quantity $(4\pi\, e\, P_{\Delta\lambda})$ is a constant for a particular wavelength λ and temperature T of the standard lamp. N is determined by reading the gas pressure, p, in microns with a McLeod gauge and then applying the relationship

$$N = 3.22 \times 10^{13}\, p \quad , \tag{31}$$

which follows from the ideal gas law and the assumption that the temperature of the gas is 300°K. The parameters Ω_{SL}, Ω_{cc}, A_{SL}, and Δx depend upon the geometry of the optical devices involved. Hence, these must be determined experimentally.

Experimental Method

The factor $\left(\frac{\Omega_{SL} A_{SL}}{\Omega_{cc} \Delta x}\right)$ in equation (30) is determined by treating

each parameter separately. To enhance one's understanding of these concepts, use will be made of Figure 8 which illustrates the geometry of the optical arrangements from a different perspective than does Figure 7.

From the magnification properties of the lens and object-image combinations, it follows that

$$A_{SL} = \frac{d_{L\ell}^2}{d_{\ell M}^2} \, WH \quad , \tag{32}$$

and

$$\Delta x = \frac{d_{b\ell}}{d_{\ell M}} \, W \quad , \tag{33}$$

when thin lens approximations are assumed.

The solid angles of the collision chamber and the standard lamp are limited by the monochromator when no external stops are used, the major limitation being the size of the grating. It is, therefore, necessary to make certain that the light entering the monochromator falls within the rectangular area of the grating. Thus, to ensure that all this light originating from either source will be detected, the following procedure is adopted. First, the top of the monochromator is removed so that the interior of the instrument may be illuminated by an external source. This permits the outline of the grating to be seen while the relatively more intense light patch appearing upon its surface and originating from either the collision chamber or the standard lamp is viewed through the exit slit. Since all the light is made to fall upon the grating surface, these precautionary steps will also minimize the effects of scattered light.

Once the illumination of the grating has been examined to ensure no light blockage within the monochromator, the effective solid angles shown

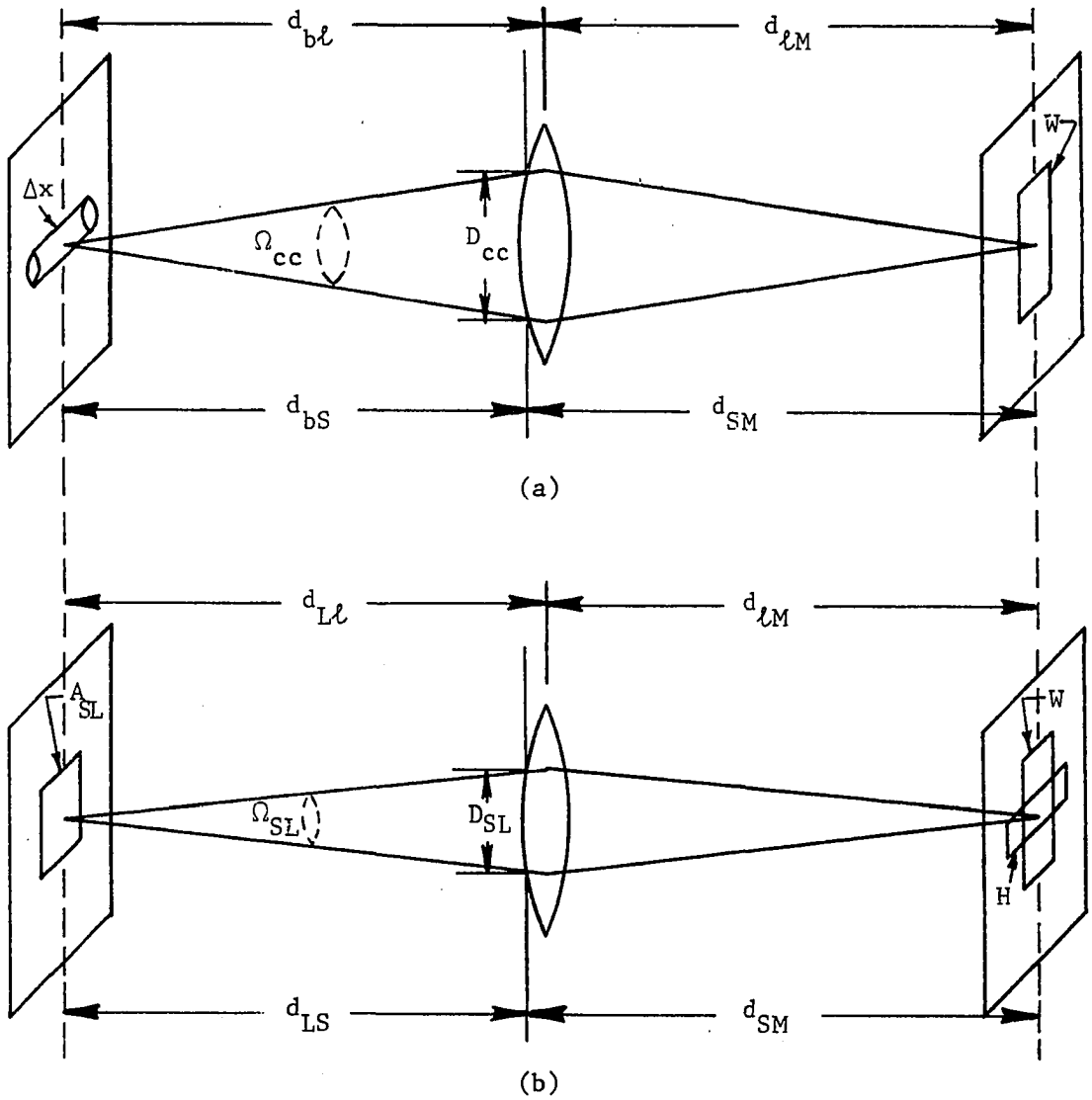

FIGURE 8. Geometry of the Optical System

(a) Collision chamber as the photon source. (b) Standard lamp as the photon source. Δx and A_{SL} are the effective length of the beam and area of the standard lamp, respectively, and Ω_{cc} and Ω_{SL} are their effective solid angles. D_{cc} and D_{SL} are the aperture stop diameters for the respective modes. The d's refer to the indicated distances where b, L, S, ℓ, and M symbolize the beam, standard lamp, aperture stops, lens, and monochromator, respectively. W is the width of the monochromator slits which are perpendicular to the beam. H is an additional slit, made from razor blades, which is added for the standardization mode in order to determine A_{SL}. Both sets of slits make physical contact with each other.

in Figure 8 may be expressed by

$$\Omega_{cc} = \frac{\pi D_{cc}^2}{4 d_{bS}^2} \quad , \tag{34}$$

and

$$\Omega_{SL} = \frac{\pi D_{SL}^2}{4 d_{LS}^2} \quad . \tag{35}$$

Equations (32), (33), (34), and (35) may now be combined to form the desired factor in equation (30). The result is

$$\frac{\Omega_{SL} A_{SL}}{\Omega_{cc} \Delta x} = \frac{H}{d_{\ell M} d_{b\ell}} \left(\frac{d_{bS} d_{L\ell} D_{SL}}{d_{LS} D_{cc}} \right)^2 \quad . \tag{36}$$

The right-hand side of equation (36) may be simplified by assuming that $d_{bS} = d_{b\ell}$ and that $d_{LS} = d_{L\ell}$. These approximations, which are equivalent to assuming that the stops coincide with the lens, introduce a calculated error which is less than .05 per cent of the true value. Therefore, under these assumptions

$$\frac{\Omega_{SL} A_{SL}}{\Omega_{cc} \Delta x} = H \frac{d_{b\ell}}{d_{\ell M}} \frac{D_{SL}^2}{D_{cc}^2} \quad . \tag{37}$$

In the actual experiment the lens was adjusted for unit magnification, i.e. $d_{b\ell}$ and $d_{\ell M}$ were set equal. Hence,

$$\frac{\Omega_{SL} A_{SL}}{\Omega_{cc} \Delta x} = H \frac{D_{SL}^2}{D_{cc}^2} \quad . \tag{38}$$

Substitution of equations (31) and (38) into equation (30) yields

$$Q_{jk} = \frac{4\pi e H P_{\Delta\lambda}}{3.22 p} \frac{D_{SL}^2}{D_{cc}^2} \left(\frac{I_{cc}}{I_e I_{SL}} \right) \times 10^{-13} \quad . \tag{39}$$

For a particular value of H, arbitrarily chosen to be .128 centimeter, the final result for Q_{jk} is

$$Q_{jk} = 8.00 \times 10^{-27} P_{\Delta\lambda} \left(\frac{D_{SL}}{D_{cc}}\right)^2 \left(\frac{I_{cc}}{I_e I_{SL}}\right) \frac{1}{p} \quad , \qquad (40)$$

where p is expressed in microns, I_{cc}, I_e, and I_{SL} are all measured in microamperes, and $P_{\Delta\lambda}$ is given by equation (29). Adjusting the ratio $\frac{D_{SL}}{D_{cc}}$ to various values permits the determination of Q_{jk} in units of cm^2 from equation (40) for any given spectral line.

CHAPTER IV

SPECTRAL CHARACTERISTICS OF NEON I

As An Inert Gas

Neon with an atomic number of ten is characterized by the ground state configuration $(1s)^2(2s)^2(2p)^6\ {}^1S_o$. Since this state is very stable a large energy is required to lift an atom to the first possible excited state which is the $(2p)^5 3s$ configuration. All the excited states of Ne I lie in the region between 16.6 and 21.6 eV from the ground state. Thus, neon has a typical series spectrum.

When one of the six 2p electrons in the outer shell is lifted to an excited level of $n \geq 3$, the excited terms will be rather hydrogen-like because the nuclear charge is now almost completely shielded by the nearly complete inner L_2 shell. On the other hand, when the six electrons are in the closed 2p shell (ground state configuration), they will be greatly influenced by the nuclear charge which is much less completely shielded. This means that the ground state will lie considerably lower than the corresponding hydrogen term (n = 2). In fact, it actually lies lower than the n = 1 term of hydrogen. The large first excitation potential coupled with the term type of the ground state of neon (^1S_o) is responsible for its character as an inert gas.

The lowest configuration of the neon ion is $(2p)^5$. This gives rise to an inverted ^2P state with a doublet separation of 780 cm^{-1}.

Thus, the excited states of neutral neon are built partially upon the lowest $^2P_{3/2}$ state or upon the 780 cm^{-1} higher $^2P_{1/2}$ state of the ion. This division of the series into two groups of levels is due to the spin-orbit interaction of the almost closed (2p) shell. This interaction is quite large and practically constant for all configurations. The spin-orbit interaction of the excited electron and the electrostatic interaction between this electron and the $(2p)^5$ core, however, decreases very rapidly as n increases. This effect gives the higher configuration members the appearance of doublets.

Types of Coupling

In order to analyze an atomic system such as that of neon and to make predictions pertaining to its internal structure, spectrum, etc., it is necessary to adopt some type of coupling scheme for the various angular momentum vectors. The more familiar Russell-Saunders- or LS-coupling, which is adopted in the case of helium, can be significantly assigned in only a few cases for the Ne I system, in particular, for any s-level but only those p-levels whose principal quantum number is n = 3. In these limited cases the excited states may be designated as is the case in helium by singlet and triplet configurations. Nearly all configurations show extreme jj-coupling. The states are not, however, in pure jj-coupling for although the j_c value of the $(2p)^5$ core is a very good quantum number, it turns out that the j_{ee} value of the excited electron is in general not a good quantum number. Consequently, neither the LS- or jj-coupling notation is adopted to describe the states of the Ne I atomic system, but rather a scheme first suggested by Racah[6]. This scheme, referred to as $j\ell$-coupling, is characterized by the following set

of equations:

$$\vec{j}_c = \vec{L}_c + \vec{S}_c \quad , \tag{41a}$$

$$\vec{K} = \vec{j}_c + \vec{\ell}_{ee} \quad , \tag{41b}$$

$$\vec{J} = \vec{K} + \vec{s}_{ee} \quad , \tag{41c}$$

where c and ee refer to the $(2p)^5$ core and excited electron, respectively. In this scheme, as can be seen from the above equations, two basis assumptions are made:

(1) the $(2p)^5$ core is bound more tightly to itself than to the excited electron, and

(2) the spin-orbit interaction of the excited electron is less significant than is that of the orbital motion of this electron with the $(2p)^5$ core.

In the case of neon the only selection rule for dipole radiation which may be rigorously applied to predict an electronic transition in the atom is

$$\Delta J = 0, \pm 1 \quad , \tag{42}$$

where a $0 \rightarrow 0$ transition is forbidden. Besides condition (42), other selection rules hold when an arbitrary atom obeys pure $j\ell$-coupling. Thus, it follows that the complete neon problem can be solved only through application of some intermediate type of coupling system.

Spectral Notation

There are currently two distinct notations used in the literature to describe a given atomic state of neon. The first of these is adopted in the $j\ell$-coupling scheme. In this notation a state is completely specified by writing it symbolically in the form

$$n\ell_{ee}^{(')} \quad K_{J}^{(o)}$$

where the prime or unprime symbol tells whether the excited electron has been coupled with the $^2P_{1/2}$ state or the $^2P_{3/2}$ state of the ion core respectively, and the (o) tells whether the state has odd or even parity.

The second notation was adopted by Paschen[7,8,9] when he made the first extensive analysis of the neon spectrum. Although the spectrum is very complex, Paschen was able to arrange it into different series which he classified and later found to be combinations between four series of S terms, ten series of P terms, 12 series of D terms, and 12 series of F terms. Since these terms were observed to combine with each other like the s, p, d, and f terms in the alkalies, Paschen named the four series of S terms s_2, s_3, s_4, and s_5, the ten series of P terms p_1, p_2, p_3, ..., and p_{10}, and the 12 series of d terms s_1', s_1'', s_1''', s_1'''', d_1', d_1'', d_2, d_3, d_4, d_4', d_5, and d_6. The letters U, V, X, Y, and Z have been used to designate the 12 series of F terms.

Although Paschen's work was accomplished long before the structure of the neon atom was understood from a quantum mechanical point of view, even today spectroscopists prefer his notation over that of the $j\ell$-scheme despite the fact that the former is perhaps less meaningful. The Paschen notation as well as his identification of the spectral lines have been used exclusively by this author. An energy level diagram of neon I is displayed in Figure 9 where the classification of states is given in both the Paschen notation and the configuration notation, the latter being written just below each $n\ell$ family.

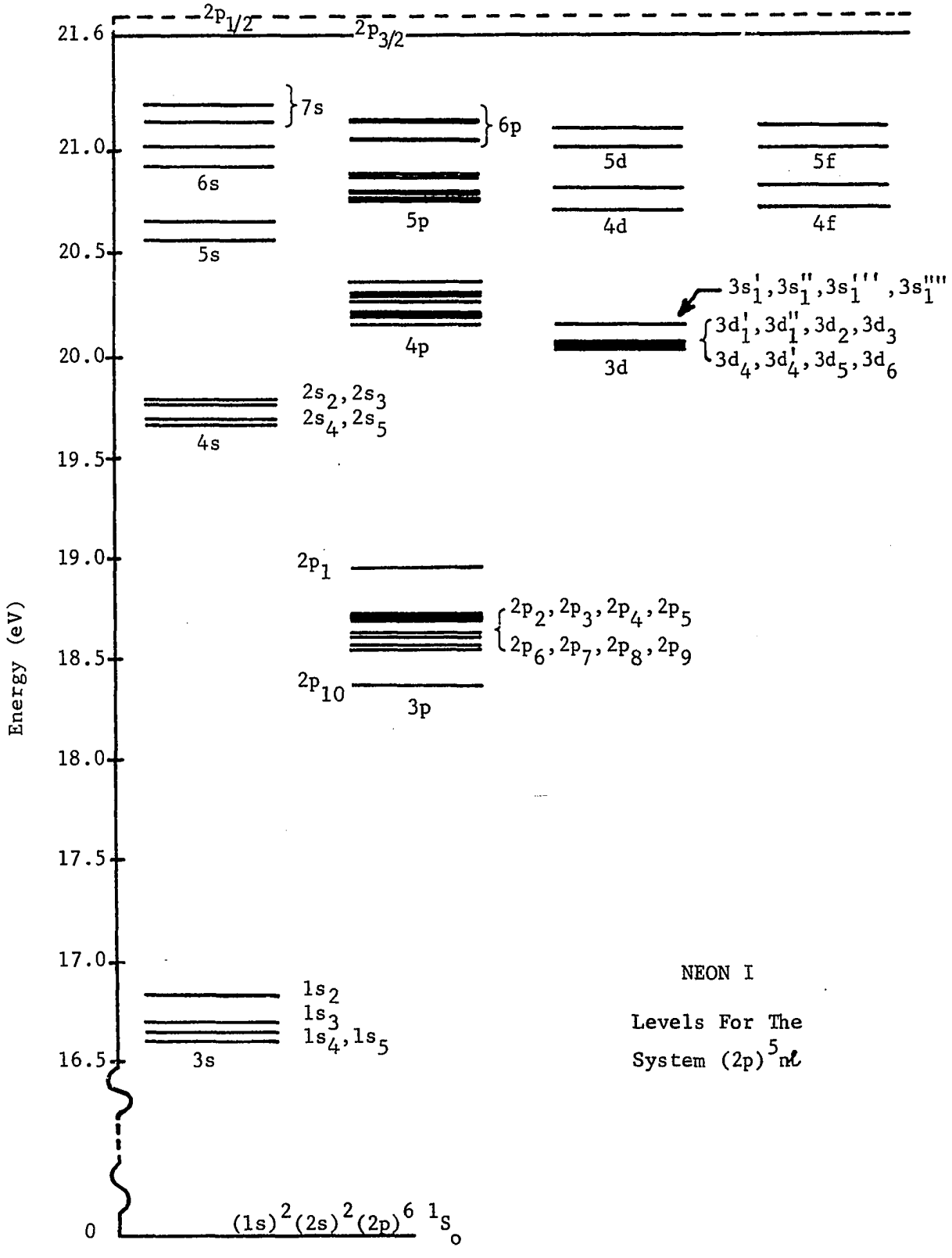

FIGURE 9. Energy Level Diagram of Neon I

CHAPTER V

APPARENT EXCITATION CROSS SECTIONS OF THE np AND ns FAMILIES

The 2p Family

By the techniques discussed previously the apparent excitation cross section of all ten 2p levels of neon have been measured over a range of energy from threshold to 200 eV. These results were obtained under conditions of low electron beam currents and atomic number densities, e.g., $I_e \leq 500$ microamperes and $N \leq 6 \times 10^{14}$ atoms/cm^3. Since optical transitions from the p levels to the ground state are forbidden by the selection rules of electric dipole radiation, one would not expect these levels to show radiation imprisonment. However, to make certain that only single electron-atom collisions were producing the excitation of the neon atoms, control experiments have been carried out to determine the relationship between the light output as a function of pressure and beam current for the ten most prominent transitions connecting the $2p \rightarrow 1s$ levels. The results of the experiments, illustrated in Figure 10 for the $2p_9$ upper level, showed that the light output always varied linearly with beam current at constant pressure or with pressure at constant beam current for the range of currents and pressures used in this application. Thus, the cross sections of the spectral lines

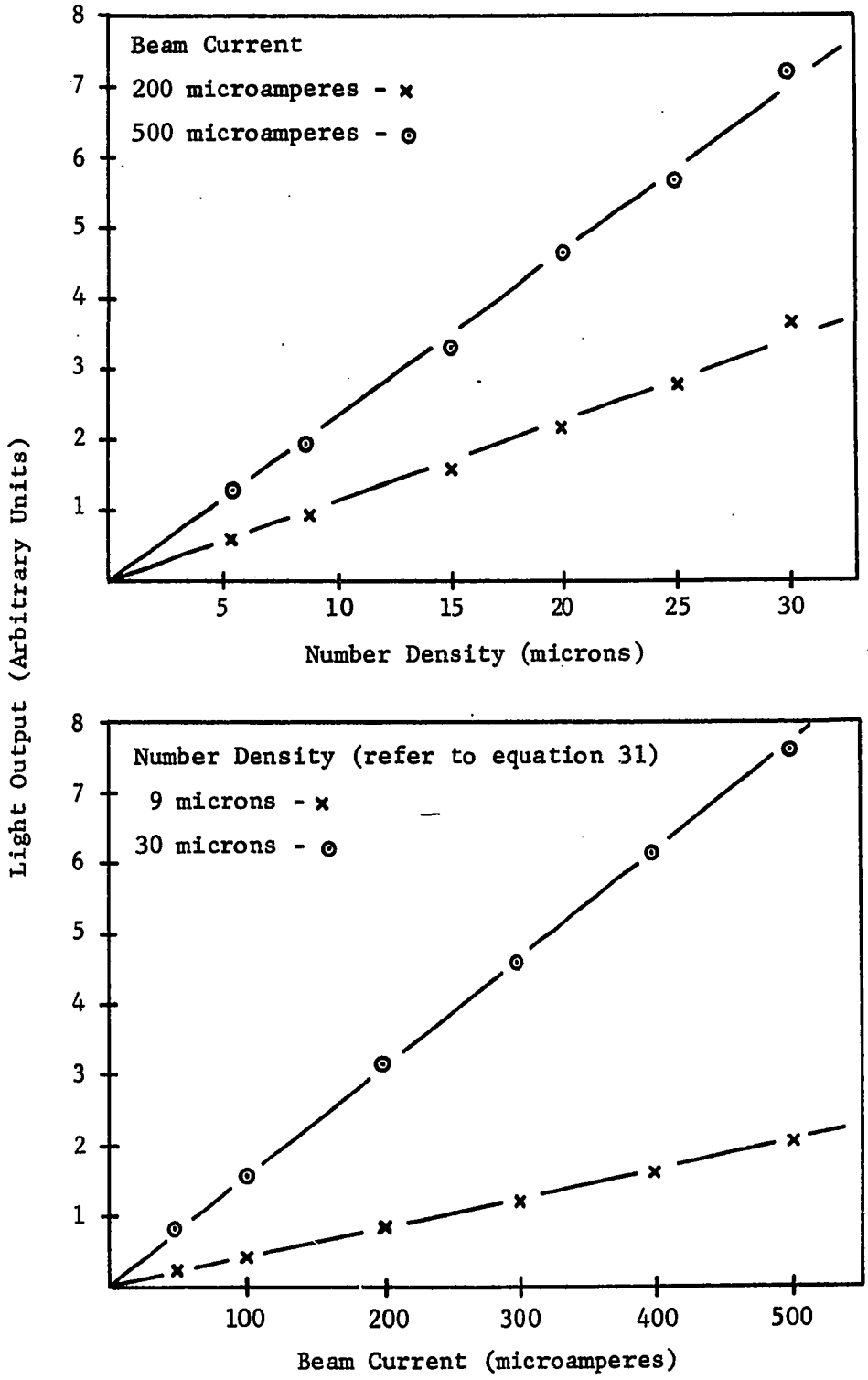

FIGURE 10. Control Experiments - $2p_9 \rightarrow 1s_2$ (100 eV)

associated with the 2p→ 1s levels and reported in this work are independent of electron beam current and atomic number density. This effectively rules out the existence of secondary processes such as imprisonment of resonance radiation and transfer of excitation collisions.

When plotting the excitation functions, a discrepancy of approximately 2 eV was observed between the theoretical and experimental onset potentials. This shift of the experimental onsets to potentials larger than those predicted by theory have been explained by Jongerius[10] to be due to the influence of space charge, contact potentials, and field penetration into the Faraday cage of the electron gun. The excitation functions presented in this work have all been adjusted so that the experimental onset potential coincides approximately with the theoretical value.

The excitation functions displayed in Figures 11 and 12 illustrate how the apparent cross sections of the ten 2p levels of neon vary from onset to 200 eV. These curves have been classified according to the total J value of the upper level, i.e. whether this quantity is an even or odd number. It has been observed by numerous investigators, e.g. in the case of helium, that pure triplet states are generally represented by excitation functions which possess a sharp peak near their onset and decline very rapidly at higher energy. The excitation function for the $2p_9$ level may indeed be described in this manner. Inspection of the Clebsch Gordon coefficient relations reveals that this state is the only one of the 2p family that is of pure triplet character. The remaining excitation functions of the 2p family all possess rather broad peaks occurring from 38 to 90 eV, the most extreme case being the curve corresponding to the $2p_3$ level. In spite of the

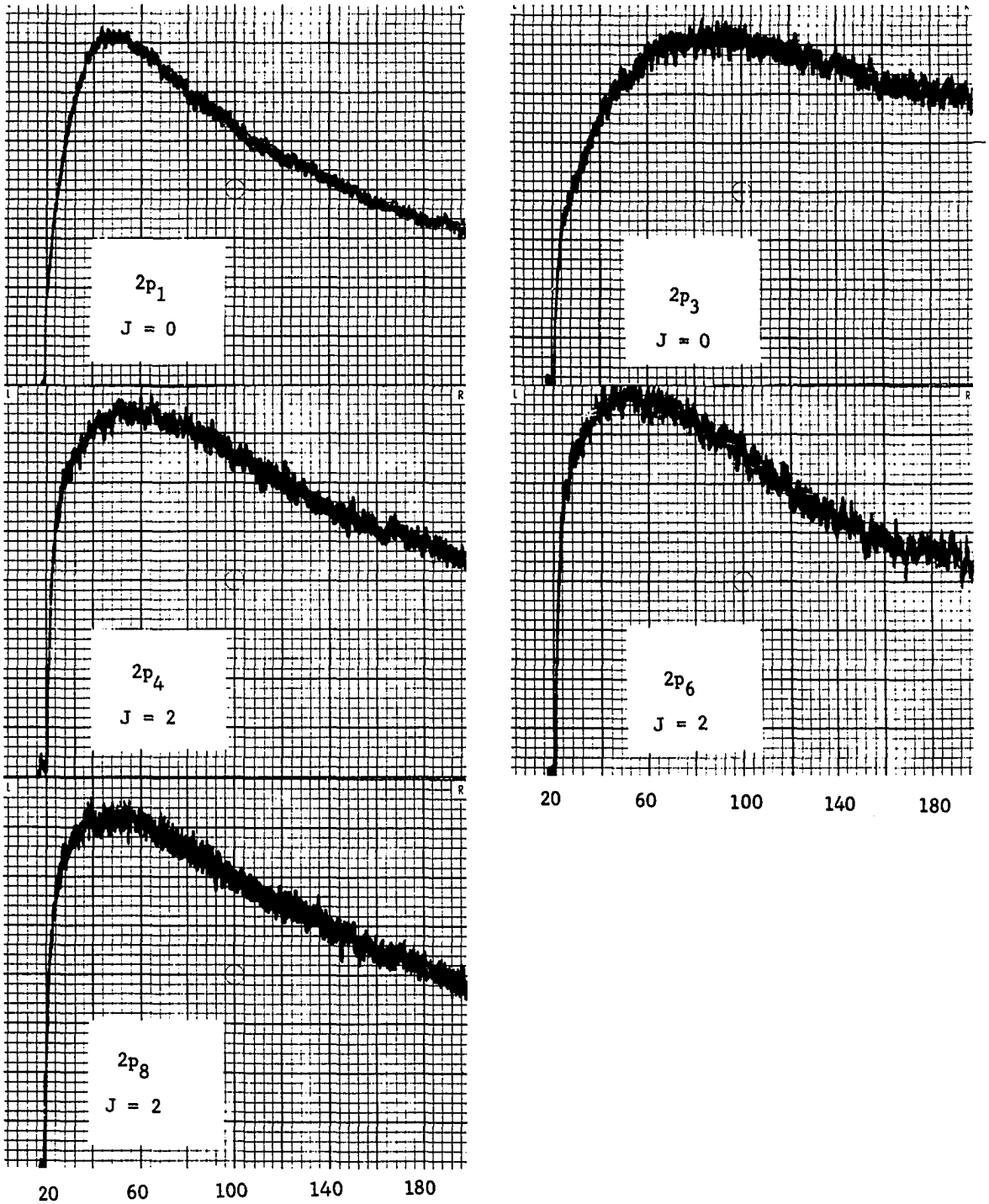

FIGURE 11. Excitation Functions of the 2p Family With Even J Values

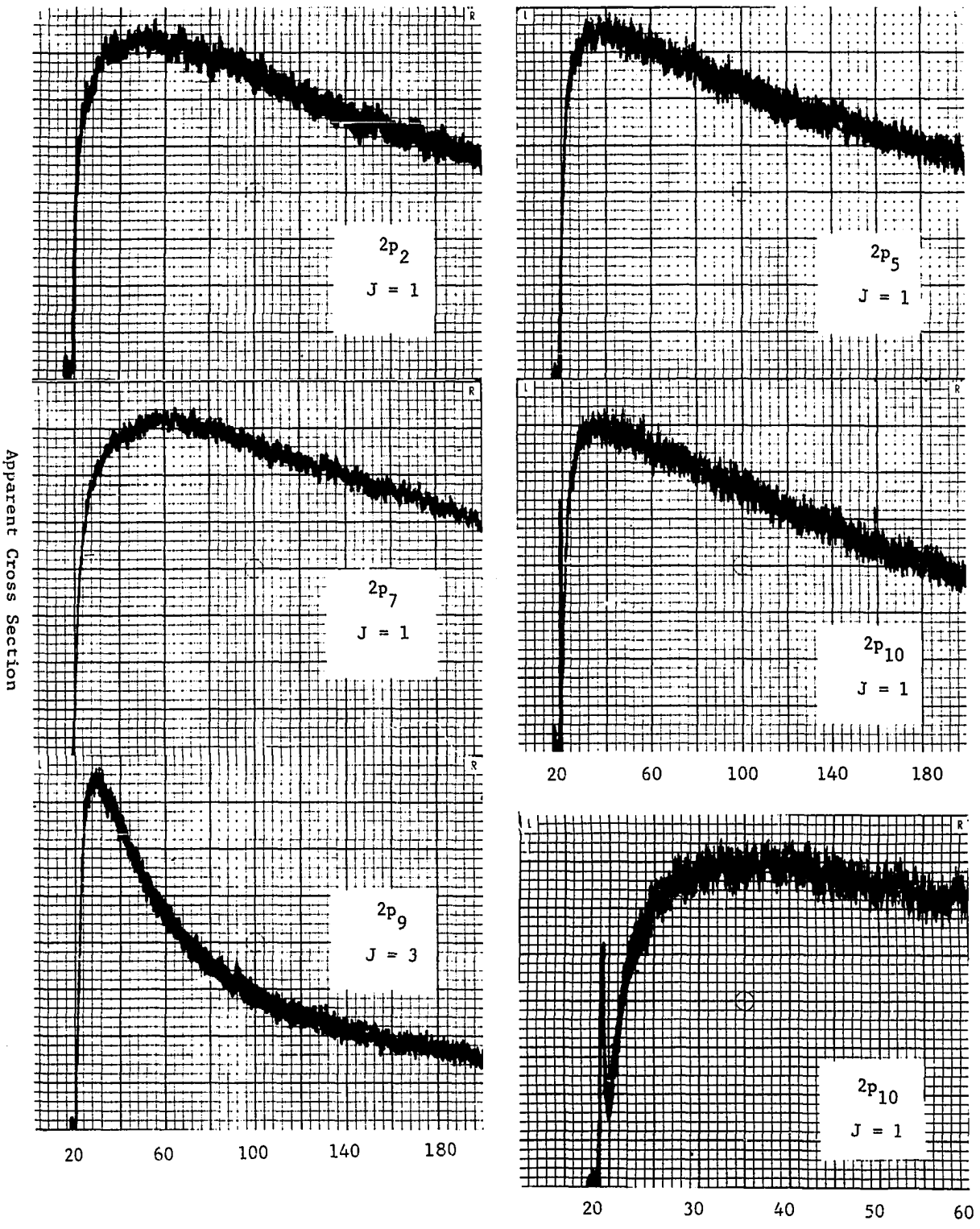

FIGURE 12. Excitation Functions of the 2p Family With Odd J Values

slight variation in the shapes these curves possess striking similarities to the excitation functions found in helium.

An additional very interesting feature was found to exist in the excitation function of the $2p_{10}$ level. Here a very sharp peak occurring at 19 eV and preceding the much broader maximum at 38 eV was obtained in this curve. The exact explanation of this added feature is not certain since the energy distribution ($\sim$0.5 eV) of the incident electrons around 20 eV seems to affect the shape of this initial spike. However, in view of recent interest by numerous investigators[11-14] in resonance and its effect in producing sharp peaks in the excitation functions, it is tempting to ascribe the sharp peak in the excitation function of the $2p_{10}$ level to this phenomenon. A few comments may be given in connection with this supposition:

(1) At first sight one may assign the sharp peak to the direct excitation function of the $2p_{10}$ level and the secondary peak primarily to cascade into this level. This, however, would imply a very sharp and narrow triplet type of excitation function. Since no other cases, not even in helium, have been reported where triplet type functions had this shape, the assumption that this is the direct excitation function would be inconsistent with all known presently existing data.

(2) The energy level spacing between the $2p_{10}$ and all the other 2p levels is of the order of 0.2 eV. This energy gap may possibly be large enough to permit at least a partial resolution (in electron energy) of the fine structure produced by the formation of Ne^- associated with the upper 2p levels.

(3) The $2p_9$ through $2p_3$ levels are all clustered closer together with

energy gaps of the order of 0.05 eV between adjacent levels. Obviously since the energy distribution of the incident electrons is much larger than this figure, one would not expect to resolve the resonance fine structures even if they do exist.

(4) The $2p_2$ to $2p_1$ energy gap is 0.24 eV. Since this is larger than the $2p_{10}$ to $2p_9$ gap, one would expect the excitation function for the $2p_2$ level to also possess a sharp spike similar to that found in the excitation function of the $2p_{10}$ level. This, however, was not the case. Therefore, this point should be investigated further.

(5) Finally, the energy spacing of the $3p_{10}$ to $3p_9$ levels is much smaller than is that of the $2p_{10}$ to $2p_9$. Thus, it is not too surprising that no evidence was found of resonance phenomenon in the $3p_{10}$ case. Nevertheless, we must emphasize at this stage that the assignment of the sharp spike found in the excitation function of the $2p_{10}$ state to the resonance behavior is a very tentative one and that additional work must be done to clarify this point.

The problem of distortion in the excitation functions as reported by Anderson et al[1] for the case of mercury due to the presence of Hg II spectral lines which could not be resolved from the desired Hg I transition was not so severe in the case of neon. Two reasons may be proposed as to the failure in finding any trace of Ne II in the excitation studies of the 2p levels: (1) the ionization cross section of Ne II is much smaller than that of Hg II, and (2) the only known Ne II lines have been found in a spectral region which lies at shorter wavelengths than those of the principal spectral lines connecting the 2p-family. As will be pointed out later, a few cases in which Ne II lines tended to distort the excitation functions did occur in the studies of

the 3p levels. The difficulty in obtaining sufficient resolution between adjacent Ne I lines, however, did present a problem as was the case in mercury. This difficulty occurred for only a few cases in the measurement of the cross sections of the transitions connecting the $2p \rightarrow 1s$ levels; in fact, the excitation functions displayed in Figures 11 and 12 were obtained by measuring the radiation emitted from spectral lines which were well isolated, the worst case being $\sim 6\text{Å}$, from any adjacent line of significant intensity. This difficulty, however, became quite severe when measurements were made to determine the percentage of cascade contributing to the apparent cross sections of the 2p levels and will be discussed in the following chapter.

The absolute cross sections of all 30 transitions originating from the 2p levels were experimentally measured at an incident electron energy of 100 eV. From this data the apparent cross sections of all ten levels have been obtained at this energy by merely summing the cross sections of all transitions originating from a common upper level. The results, grouped according to the respective levels involved, are presented in Table 1. Also tabulated for convenience and future reference are the wavelengths of the corresponding spectral lines. With the aid of the excitation functions displayed in Figures 11 and 12 the apparent cross section of any 2p level from onset to 200 eV may be obtained by merely multiplying the relative height of the respective curve by the value of its corresponding cross section at 100 eV.

The limits placed upon the experimental errors were based solely upon the experimental repeatability, i.e. independent cross section determinations at different times, for various beam currents and gas pressures within the range previously specified, and for different

TABLE 1. Absolute Cross Sections of the Spectral Lines for the Series $2p \rightarrow 1s$

The upper number in each entry is the value of Q_{jk} at 100 eV in units of 10^{-20} cm^2 and the lower number is the corresponding wavelength in Å.

	$2p_1$	$2p_2$	$2p_3$	$2p_4$	$2p_5$	$2p_6$	$2p_7$	$2p_8$	$2p_9$	$2p_{10}$
$1s_2$	168±11 5852	18±3 (6599)[C]	0.24 ±0.05 6652	43±6 (6678)[C]	19±2 (6717)[C]	35±4 6929	1.9±0.5 7024	5.9±0.7 7174	——	0.86 ±0.30 8082
$1s_3$	——	10±2 (6164)[C]	——	——	19±3 6266	——	11±2 6533	——	——	3.2 ±0.5 7439
$1s_4$	1.9±0.3 5401	4.1±0.5 6030	37±6 6074	33±4 6096	0.7±0.1 6128	7.8±1.3 6305	35±6 6383	53±8 6507	——	13±1 7245
$1s_5$	——	8.9±0.9 5882	——	19±3 5945	3.2±0.6 (5976)[C]	53±8 (6143)[C]	7.0±1.2 6217	28±4 (6334)[C]	35±6 (6402)[C]	33±3 7032
$\sum_{1s} Q_{jk}$	170±11	41±6	37±6	95±13	42±6	96±13	55±10	87±13	35±6	50±5

[C]The indicated spectral line could not be completely resolved from an adjacent less intense one. Therefore, adjustments were made by employing theoretical branching ratios.

temperatures of the standard lamp. An error analysis was made of the measuring devices, e.g. the electron beam current meter, the Lock-In amplifier, the chart recorder, the McLeod gauge, and the standard lamp current monitor. Consideration was even given to the scattering of the standard lamp light within the monochromator for some regions of the spectrum. Only the uncertainties in the standard lamp ribbon, e.g. the emissivity of tungsten and the calibration of the true temperature, were excluded in the consideration of factors which were believed would introduce errors into the cross section measurements determined from equation (40). This analysis resulted in an estimate of the probable experimental error which was less than the general repeatability of the experimental measurements. Thus, it was decided that the most logical method of determining the experimental error was to perform the experiment several times (at least six), average the results, and then use the extreme values as the limits.

Comparisons with Other Investigators

As previously stated very little known experimental excitation data exists for neon. Up to this time the most significant contribution had been made by Hanle[15] in 1930 and by Herrmann[16] in 1936. Hanle's results consist essentially of 16 distinct excitation functions for spectral lines of the $2p \rightarrow 1s$ series over an energy range from threshold to 100 eV. No report was given in his paper of the absolute intensity at a given energy of these lines. Hence, one can only obtain relative data from this paper. Herrmann, on the other hand, published no excitation functions of neon. His work consisted in measuring the absolute cross section of only 14 spectral lines belonging to the $2p \rightarrow 1s$ series and three lines cascading into the $2p_5$ and $2p_9$ levels. A

comparison is given below in Table 2-a of Herrmann's results with those of this work for the maximum values of those cross sections which were reported by him. The relative shapes presented by Hanle and the absolute data presented by Herrmann appear to agree quite well with the results of this work when one considers that they both used photographic plates in contrast to photomultiplier tubes to detect the radiation emitted from the collision region.

Subsequent papers on work pertaining to spectral lines belonging

TABLE 2-a. Experimental Comparison of the Excitation Cross Section for Some Spectral Lines of the $2p \rightarrow 1s$ Series

The Q_{jk}'s, given in units of 10^{-20} cm^2, are the maximum values of the respective cross sections.

Wavelength in Å	Transition	$Q_{jk}(max)$ This Work	Herrmann
5852	$2p_1 \rightarrow 1s_2$	225± 15	172
5945	$2p_4 \rightarrow 1s_5$	21± 3	19
6074	$2p_3 \rightarrow 1s_4$	38± 6	29
6096	$2p_4 \rightarrow 1s_4$	37± 4	30
6143	$2p_6 \rightarrow 1s_5$	63± 9	69
6217	$2p_7 \rightarrow 1s_5$	7.5± 1.3	12
6266	$2p_5 \rightarrow 1s_3$	22± 4	27
6334	$2p_8 \rightarrow 1s_5$	34± 5	38
6383	$2p_7 \rightarrow 1s_4$	38± 6	39
6402	$2p_9 \rightarrow 1s_5$	91± 16	90
6507	$2p_8 \rightarrow 1s_4$	64± 10	65
6678	$2p_4 \rightarrow 1s_2$	48± 7	72

to the $2p \rightarrow 1s$ series are:

(1) a report on the absolute excitation cross sections of four prominent lines at an incident electron energy of 100 eV by Milatz and Woudenberg[17] in 1940,

(2) the determination of the absolute maximum value of the cross sections for 23 spectral lines by Frish[18], and

(3) a publication by Zapesochnyi and Fel T San[19] displaying three excitation functions of very prominent spectral lines.

The latter paper is the result of a study of neon using a highly monoenergetic electron beam. The general features of the three resulting curves resemble very closely the excitation functions of the $2p_1$, $2p_4$, and $2p_9$ levels displayed in Figures 11 and 12. There are, however, secondary peaks in the curve corresponding to the $2p_1$ level.

Milatz, using photographic plates, measured only four lines which were previously measured by Herrmann. Frish's work is the result of measurements made in a positive column of a D.C. discharge which are different conditions than those of this work. In view of these conditions under which their data was obtained, any attempt to compare the results presented in this paper with the findings of Milatz and Frish is felt to be of little value.

In order to compare experiment with theory, the experimental cross sections given in Table 1 have been converted to experimental branching ratios and the results are given in Table 2-b. Also given in this table for comparison are a few experimental branching ratios which were calculated from transition probabilities reported by Irwin and Nodwell[20] and theoretical branching ratios obtained from the theoretical transition probabilities calculated by Fred E. Fajen[2]. The general

TABLE 2-b. Comparison Between Experiment and Theory of Branching Ratios*
for the Atomic Transitions Belonging to the $2p \rightarrow 1s$ Series

The upper number in each entry is a result of this work.

	$2p_1$	$2p_2$	$2p_3$	$2p_4$	$2p_5$	$2p_6$	$2p_7$	$2p_8$	$2p_{10}$
$1s_2$	1.0 $(1.0)^T$	2.3 $(2.3)^E$ $(2.6)^T$	150 $(81)^T$	2.2 $(2.1)^E$ $(4.6)^T$	2.2 $(2.1)^T$	2.7 $(2.7)^E$ $(1.7)^T$	29 $(420)^T$	15 $(13)^E$ $(38)^T$	58 $(200)^T$
$1s_3$	—	4.1 $(3.7)^E$ $(3.8)^T$	—	—	2.2 $(3.1)^T$	—	5.0 $(2.9)^T$	—	16 $(14)^T$
$1s_4$	90 $(48)^T$	10 $(11)^E$ $(10)^T$	1.0 $(1.0)^T$	2.9 $(3.1)^E$ $(3.1)^T$	60 $(11)^T$	12 $(13)^E$ $(31)^T$	1.6 $(1.8)^T$	1.6 $(1.8)^E$ $(1.5)^T$	3.9 $(3.8)^T$
$1s_5$	—	4.6 $(4.8)^E$ $(4.1)^T$	—	5.0 $(4.8)^E$ $(2.2)^T$	13 $(8.7)^T$	1.8 $(1.8)^E$ $(2.8)^T$	7.8 $(12)^T$	3.1 $(2.8)^E$ $(3.1)^T$	1.5 $(1.5)^T$

*The $2p_9$ level has been omitted from this table since the $2p_9 \rightarrow 1s_5$ transition always yields a branching ratio of 1.0.

^{E}Calculated from experimentally measured transition probabilities by J. C. Irwin and R. A. Nodwell.

^{T}Calculated from theoretical transition probabilities supplied by Fred E. Fajen.

agreement is quite good for the more probable transitions but large discrepancies exist for those spectral lines of low intensity. Not all the discrepancy can be attributed to the theory at this point for it is reasonable to believe that there will be more uncertainty in the experimental values for weak transitions than for stronger ones. However, for those cases where the theory and the experiment of this work depart noticeably, and yet the spectral lines involved are relatively intense, it appears that the two experimental values agree in cases where they can be compared more closely than do those between experiment and theory.

Looking at the neon problem as a whole and comparing the agreement here with that found in mercury by Anderson[3], one would have to conclude that the theoretical picture of the neon atom is quite good.

The 3p Family

In order to see how the cross section versus energy changes as the n value is increased the 3p family of levels were studied. Greater care had to be exercised in order to obtain the set of excitation functions displayed in Figures 13 and 14 than was necessary for the corresponding curves of Figures 11 and 12 of the 2p family. This was due to the following two factors:

(1) Since the 3p levels are more closely spaced than are the corresponding 2p ones, greater resolution was required from the monochromator. This meant it was necessary that the slit jaws be separated ~0.10 millimeters for some cases in order to separate the spectral lines. The loss of intensity resulting from this requirement, added to the already less intense $3p \rightarrow 1s$ transitions because of higher n value, presented an indeed difficult situation

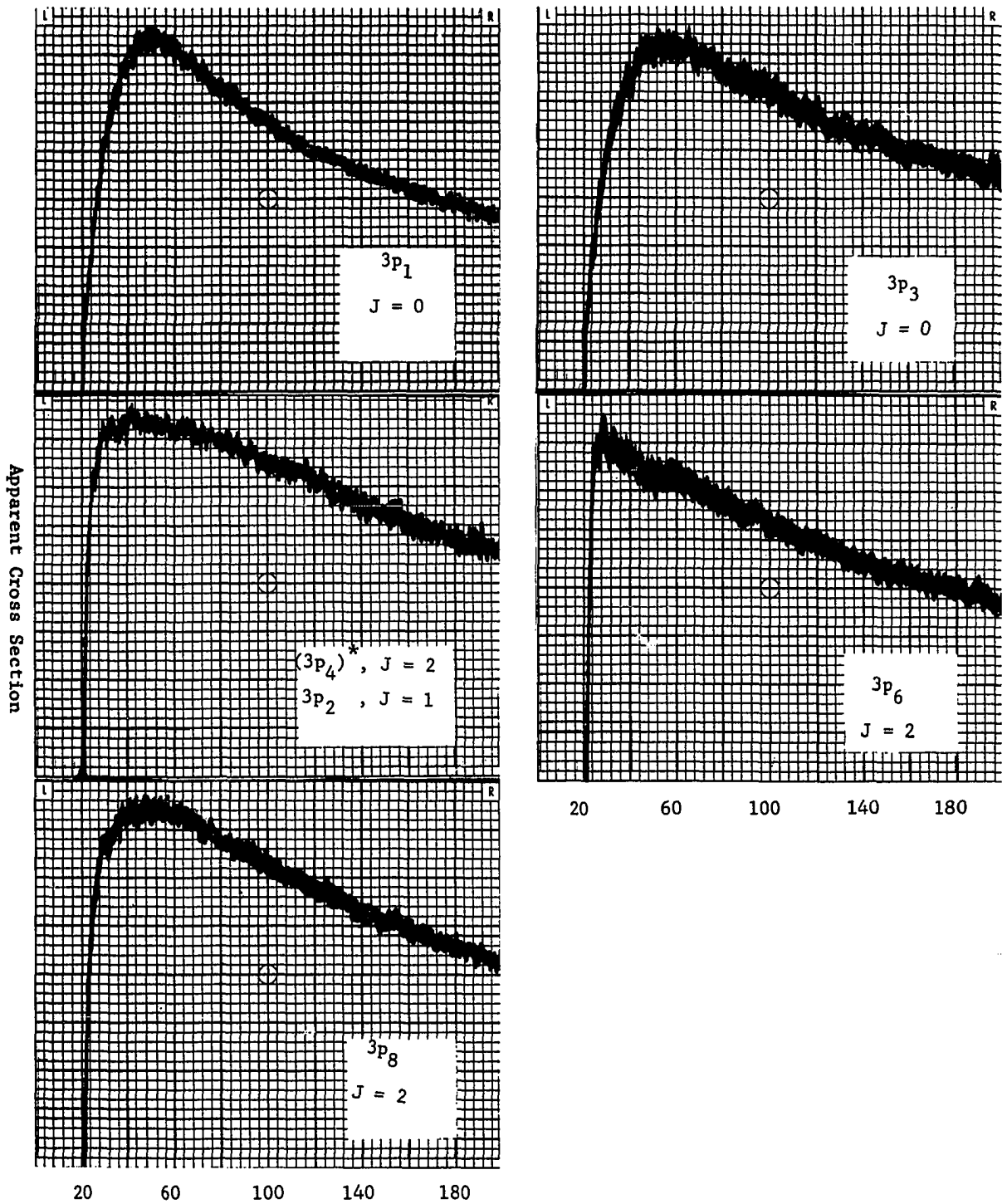

FIGURE 13. Excitation Functions of the 3p Family With Even J Values

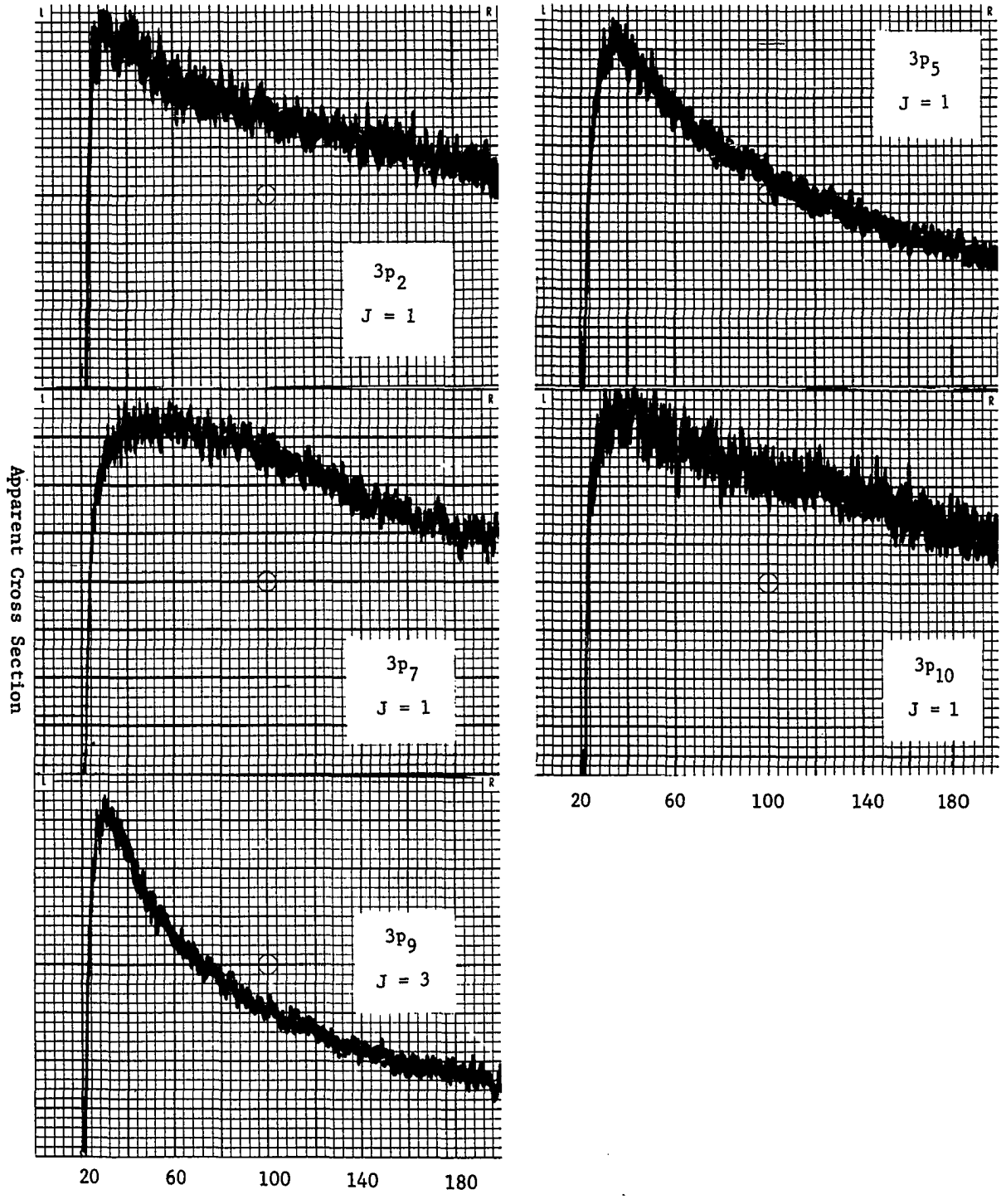

FIGURE 14. Excitation Functions of the 3p Family With Odd J Values

in the $3p_2$ and $3p_{10}$ case as may be noted from the rather noisy curves shown in Figure 14 for these levels. Despite these precautions, it was found experimentally impossible to separate the spectral lines associated with the $3p_4$ level from those of the $3p_2$ level since in all three instances the transitions were within 0.112 Å of each other. Thus, the excitation function displayed in Figure 13 is the sum of the apparent cross section of the $3p_4$ and $3p_2$ levels. From the results obtained for the corresponding transitions in the $2p_2$ and $2p_4$ case it is assumed that the radiation emitted from the $3p_4 \rightarrow 1s_4$ transition which this curve represents is much more intense than that of the $3p_2 \rightarrow 1s_4$ transition. Thus, this curve as the asterisk (*) indicates represents primarily the apparent cross section of the $3p_4$ level.

(2) The second factor contributing to the difficulty of obtaining the excitation functions of the 3p family was due to the presence of Ne II lines which rather thickly populate this region of the Ne I spectrum and, hence, tend to distort the shape of the curves at higher energy. Hence, $3p \rightarrow 1s$ transitions had to be chosen which were sufficiently isolated from neighboring Ne II spectral lines so that adequate intensity could be obtained to permit realistic plotting of the desired excitation function. All the curves shown are free of any known Ne II contaminating lines.

Comparing the excitation functions of the 3p family with the corresponding 2p ones illustrates which levels are most significantly affected by cascade as the energy of the electron beam is varied. Most of the 3p curves retain the general shape of their 2p counterpart. The curves showing significant change are those corresponding to the $3p_2$, $3p_3$, $3p_5$,

and $3p_6$ levels. These curves have sharper peaks shifted toward lower energy and their tails decline faster with increasing energy than do their 2p counterparts. These levels show the effects of a decrease in the cascade contribution as n changes from 2 to 3. Of these four levels the $3p_3$ illustrates this concept most significantly. Since it is fed by five levels for each n value (ns_2, ns_4, ns_1', nd_2, and nd_5 all of which are broad, having their maximum around 100 eV), it is not too surprising to see that when the $2s_2$, $2s_4$, $3s_1'$, $3d_2$, and $3d_5$ levels are excluded from the cascade contribution the shape of the $2p_3$ excitation function will take on a form which should look like that of the $3p_3$ level. Of these four levels the $3p_3$ is the only one that is fed exclusively from upper levels possessing broad excitation functions. Therefore, the less significant change in the excitation functions of the $3p_2$, $3p_5$, and $3p_6$ levels in going from their 2p counterparts may be ascribed to the fact that they are fed not only by upper levels possessing broad excitation functions but also by upper levels having narrow (triplet type) excitation functions as well. However, inspection of the cascade at 100 eV (the results of which will be given later) into the $2p_3$ level shows that the major contribution is from those levels possessing broad excitation functions. Thus, the sharper peaks and the faster decline of the tails in the excitation functions of the $3p_2$, $3p_5$, and $3p_6$ over the corresponding ones of the 2p family are not too surprising. Finally, the sharp spike which existed in the $2p_{10}$ excitation function was not found in the $3p_{10}$ case.

In Table 3 the absolute value of the cross section of the ten spectral lines yielding the ten 3p curves of Figures 13 and 14 are given in units of 10^{-20} cm^2 at an electron energy of 100 eV. These numbers

are used in the following chapter to obtain an estimate of the amount of cascade into the four 2s levels from the ten 3p levels.

Since this work represents the first known study of the $3p \rightarrow 1s$ series, comparison with other investigators is impossible.

The ns Families

Each ns family is composed of four energy levels. These levels, designated in the Paschen notation as ns_2, ns_3, ns_4, and ns_5, are characterized by the total J values 1, 0, 1, and 2, respectively. As previously stated the total J value of a given neon level is the only

TABLE 3. Absolute Cross Sections of the Prominent Spectral Lines Belonging to the $3p \rightarrow 1s$ Series

Wavelength in Å	Transition	Q_{jk} at 100 eV in Units of 10^{-20} cm^2
3520	$3p_1 \rightarrow 1s_2$	12± 2
3461	$3p_2 \rightarrow 1s_3$	0.4± 0.1
3454	$3p_3 \rightarrow 1s_4$	2.8± 0.6
3594	$3p_4 \rightarrow 1s_2$	(1.3± 0.3)*
3467	$3p_5 \rightarrow 1s_3$	0.7± 0.2
3448	$3p_6 \rightarrow 1s_5$	1.6± 0.3
3501	$3p_7 \rightarrow 1s_4$	1.1± 0.2
3464	$3p_8 \rightarrow 1s_5$	1.2± 0.2
3473	$3p_9 \rightarrow 1s_5$	0.9± 0.2
3511	$3p_{10} \rightarrow 1s_5$	0.2± 0.1

*The Q_{jk} value which was measured represents the sum of the transitions $3p_4 \rightarrow 1s_2$ and $3p_2 \rightarrow 1s_2$. The number presented here was scaled according to the ratio of the measured Q_{jk} values corresponding to the $2p_4 \rightarrow 1s_2$ and $2p_2 \rightarrow 1s_2$ transitions.

good quantum number resulting from any type of coupling scheme which may be employed to study the atom. This means that the total angular momentum would be a constant of the motion. Thus, one can expand the wavefunction of the state to which the level in question represents in terms of the eigenfunctions corresponding to the same J value of a given ns family described by LS-coupling. To obtain the form of this function it is necessary then to first find the form of the eigenfunctions describing the state in the LS-notation. When an s-electron is coupled with the $(2p)^5$ core the possible spectral terms which arise are $^1P_1$, $^3P_2$, $^3P_1$, and $^3P_0$. Thus, the eigenfunctions depend only on these terms. The form of the wavefunctions for the individual ns levels are then as follows:

$$\Psi_{ns_2}\ (J = 1) = \alpha u(^1P_1) + \beta u(^3P_1) \quad , \tag{43}$$

$$\Psi_{ns_4}\ (J = 1) = -\beta u(^1P_1) + \alpha u(^3P_1) \quad , \tag{44}$$

$$\Psi_{ns_3}\ (J = 0) = u(^3P_0) \quad , \tag{45}$$

and

$$\Psi_{ns_5}\ (J = 2) = u(^3P_2) \quad . \tag{46}$$

These expressions which describe the form of the wavefunction of the individual states of any ns family reveal that the ns_3 and ns_5 levels are of pure triplet character, while the ns_2 and ns_4 levels are a mixture of singlet and triplet components. As already pointed out in the $2p_9$ case, one expects pure triplet states to be characterized by excitation functions which have sharp peaks and fast declining tails at higher energy. This is indeed the case as may be seen from Figure 15b for the $3s_3$, $4s_3$, $3s_5$, $4s_5$, and $5s_5$ levels. Also, since the ns_2 and ns_4

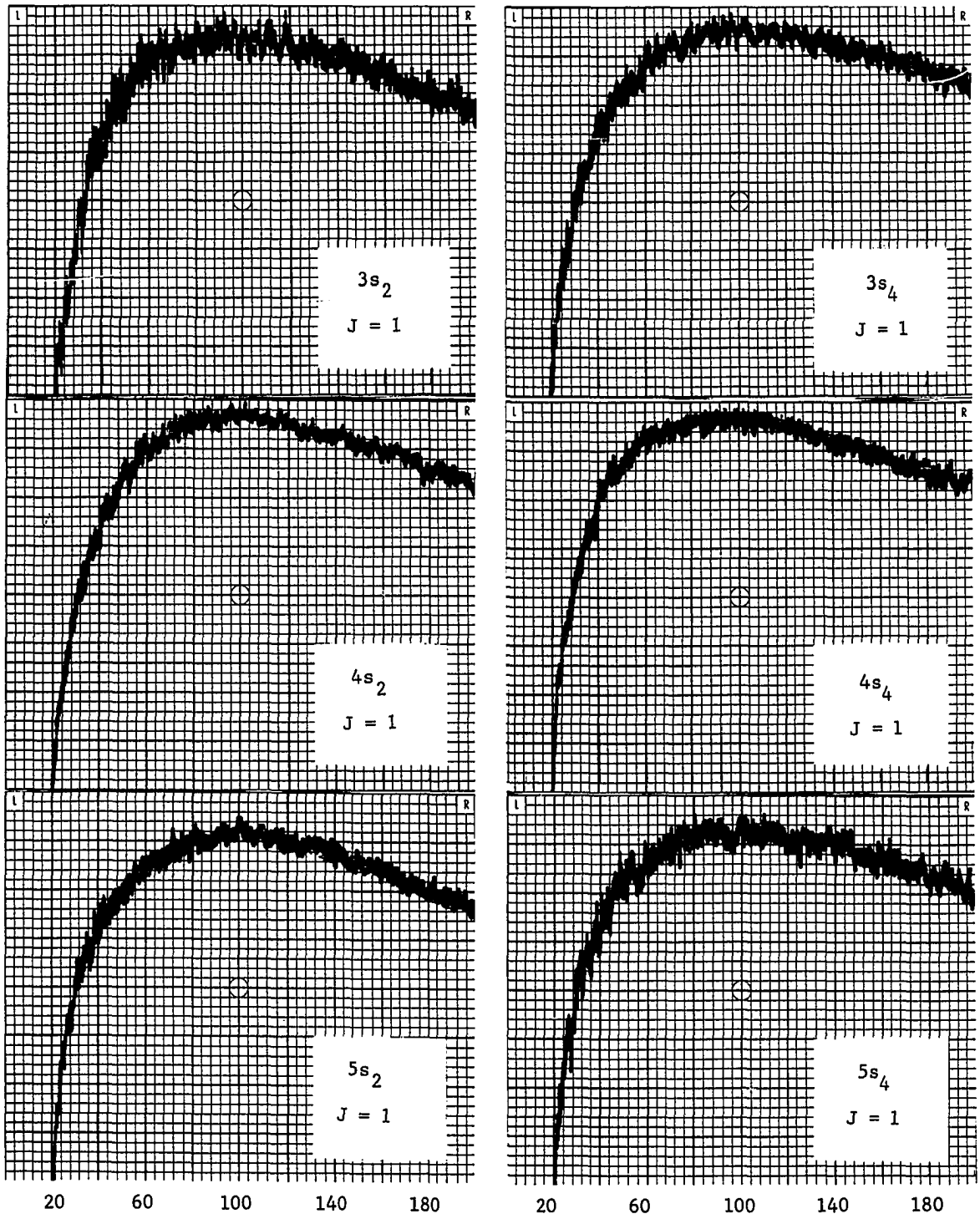

FIGURE 15a. Excitation Functions of the s Levels

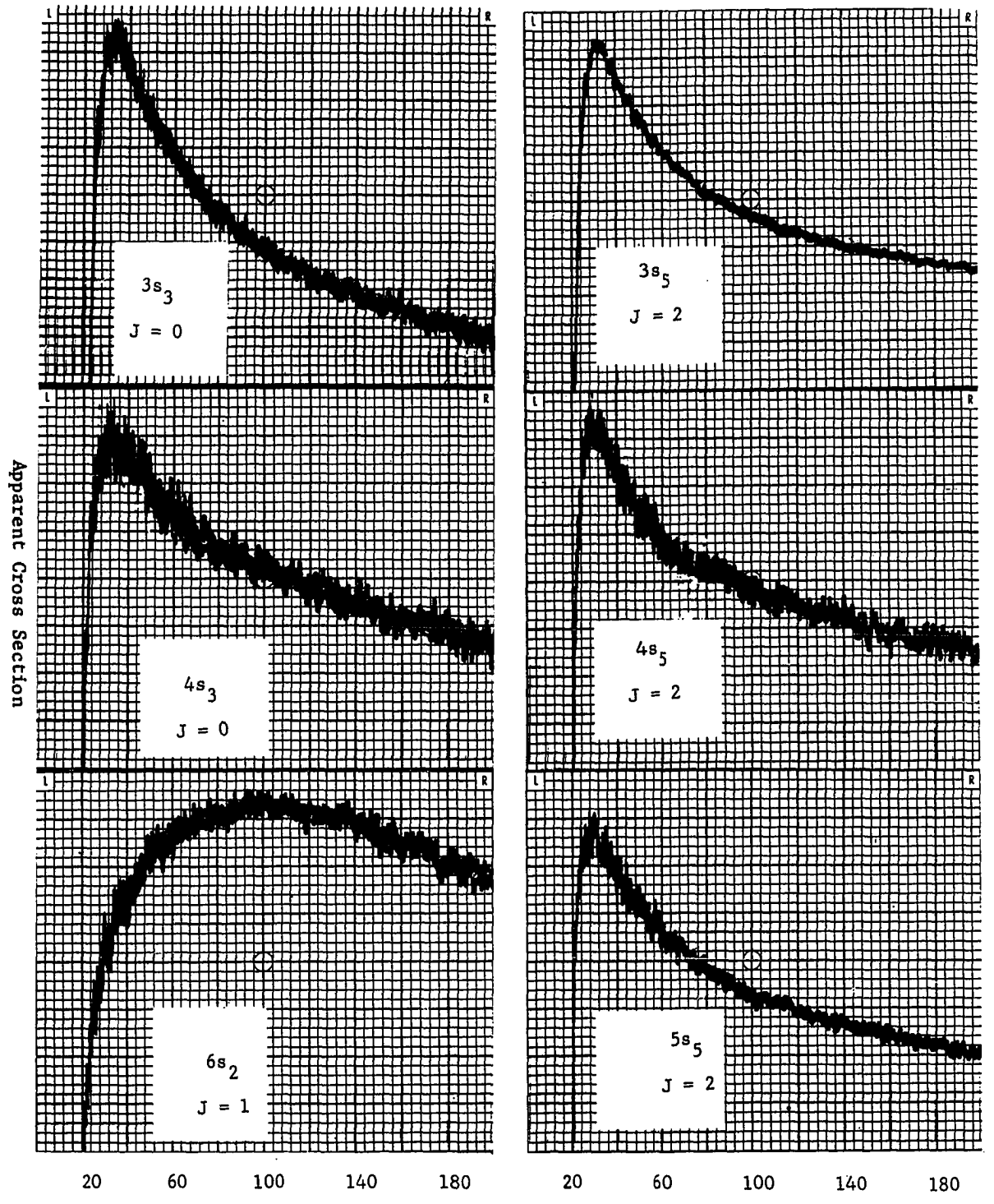

FIGURE 15b. Excitation Functions of the s Levels

levels are mixtures of singlet and triplet components, it is not too surprising to find that the shape of their excitation functions have the very broad feature illustrating that the singlet component is dominant.

The excitation functions of the s levels have the following interesting features: (1) The curves do not show any significant variation in shape with n value. Such a variation produced by a change in the cascade component with n was observed to occur in a few cases for the np families. (2) The shape of the ns_3 and ns_5 excitation functions are almost identical. The same may be said of the ns_2 and ns_4 excitation functions. (3) Finally, the curves show no resemblance to the excitation functions of the np families which cascade into them.

These three qualitative features may lead one to conclude that the s levels are not significantly affected by cascade (say less than 20 percent). This problem is studied from a quantitative aspect in the following chapter where the results are presented for the cascade contribution from the 3p family of levels into those of the 2s family. This analysis was carried out for an incident electron energy of 100 eV.

In order to draw a few analogies between neon and helium, the following results from helium are listed:

(1) Those levels having transitions connecting the ground state which are optically allowed by the selection rules of electric dipole radiation, i.e. the ^1P levels, possess very broad excitation functions. The other singlet levels (^1S and ^1D) also have broad excitation functions, i.e. broad with respect to the triplet type of curves, but they are not as broad as the excitation functions of the ^1P levels.

(2) The apparent cross sections of the singlet levels are in general much larger than those of the triplet levels having the same n value.

The first observation above for the helium case would imply that one would expect the excitation functions of the ns_2, ns_4, ns'_1, nd_2, and nd_5 levels to possess very broad peaks, even broader than those of the p levels. Inspection of the excitation functions involved reveals that this is indeed the situation.

In order to compare neon with that of helium in regard to the second observation given above, the apparent excitation cross sections for an incident electron energy of 100 eV of the 2s, 3s, and 4s families are presented in Table 8. These results were obtained by determining the cross sections of all optically allowed $j \rightarrow k$ transitions connecting the desired ns family with all lower np levels and the ground state. Thus, it was necessary to measure the cross sections of as many spectral lines as could be isolated and detected, and then from these values employ theoretical transition probabilities (listed in the Appendix) to obtain the rest. Tables 4-7 give the cross sections of all significant $j \rightarrow k$ transitions connecting the ns families with the 2p family. The data has been presented in this manner in order to illustrate more effectively the cascade analysis of the ten 2p levels presented in the following chapter. Thus, the explanation of these tables is deferred until then. The contribution to the apparent cross sections for an incident electron energy of 100 eV of the 2s, 3s, and 4s levels given in Table 8 which results from those transitions connecting the 2p family may be obtained by merely adding the Q_{jk} values of Tables 4, 5, and 6 horizontally, i.e. those values belonging to the same row.

Examination of Table 8 reveals that the apparent cross sections of

all ns_3 and ns_5 levels (the pure triplet states) are always much less than those for the ns_2 and ns_4 levels belonging to the same family. Since the values given for the ns_2 and ns_4 levels are in all three cases presented so much larger than those of the ns_3 and ns_5 levels at 100 eV, it is quite obvious that upon examination of the excitation functions presented in Figures 15a and 15b the apparent excitation cross sections of all ns_3 and ns_5 levels will be less than the corresponding values of the ns_2 and ns_4 levels for any energy. Thus, neon and helium are similar for the above two characteristics.

It should be noticed that a column of numbers has been included in Table 8 which gives the percentage of the apparent cross sections which resulted from Q_{jk} values obtained by employing theoretical transition probabilities. The figures show that in all instances theory affected more than 50 percent of the final result. Fajen* has shown that the transition probability is very sensitive to the wave functions of the upper state, at least for those transitions corresponding to spectral lines associated with the $2s_2$, $2s_4$ levels and the ground state. He has found that a slight change in the wave function of either Ψ_{2s_2} or Ψ_{2s_4} can affect the transition probability to the ground state by a factor greater than two. This result places considerable doubt upon the numerical values listed for the apparent cross sections of the ns_2 and ns_4 levels. Also, it forces one to wonder if the results are reliable for the ns_3 and ns_5 levels since the greater percentage of their apparent cross sections was obtained by employing theoretical

*Private communication with Fred E. Fajen, Los Alamos Scientific Laboratories, Los Alamos, New Mexico.

TABLE 4. Absolute Cross Sections of the Spectral Lines for the Series $2s \rightarrow 2p$

The upper number in each entry is the value of Q_{jk} at 100 eV in units of 10^{-20} cm^2 and the lower number is the corresponding wavelength in Å.

	$2p_1$	$2p_2$	$2p_3$	$2p_4$	$2p_5$	$2p_6$	$2p_7$	$2p_8$	$2p_9$	$2p_{10}$
$2s_2$	$(1.1)^T$ 15,234	$(5.5)^T$ 11,767	$(1.1)^T$ 11,602	$(9.2)^T$ 11,523	$(3.2)^T$ 11,409	9.7 ±1.9 10,845	1.3 ±0.5 10,621	$(0.9)^T$ 10,295	—	$(2.3)^T$ 8,866
$2s_3$	—	$<(0.8)^T$ 11,985	—	—	$<(1.0)^T$ 11,614	—	$<(1.5)^E$ 10,798	—	—	$<(0.6)^T$ 8,989
$2s_4$	$(0.4)^T$ 17,165	$<(0.1)^T$ $(\ )^{\ell}$	$(2.1)^T$ 12,689	$(1.1)^T$ 12,595	$(3.2)^T$ 12,459	$(5.0)^T$ 11,789	$(5.9)^T$ 11,525	20±4 11,143	—	4.2±0.9 9,487
$2s_5$	—	$(0.35)^T$ 13,219	—	$(1.3)^T$ 12,912	$(0.18)^T$ 12,767	$(1.1)^T$ 12,066	$(0.18)^T$ 11,790	$(1.4)^T$ 11,391	$(6.7)^T$ 11,178	2.7±0.8 9,665
$\sum_{2s} Q_{jk}$	$(1.5)^T$	$\sim(6.7)^T$	$(3.2)^T$	$(12)^T$	$\sim(6.6)^T$	16±3	$\sim(8.9 \pm 1.9)^{T,E}$	22±4	$(6.7)^T$	$\sim(9.8 \pm 2.0)^{T,E}$

^{T}Calculated using theoretical branching ratio.

^{E}Estimated from experimental data.

$^{\ell}$Indicated line has never been reported in the literature.

TABLE 5. Absolute Cross Sections of the Spectral Lines for the Series $3s \rightarrow 2p$

The upper number in each entry is the value of Q_{jk} at 100 eV in units of 10^{-20} cm^2 and the lower number is the corresponding wavelength in Å.

	$2p_1$	$2p_2$	$2p_3$	$2p_4$	$2p_5$	$2p_6$	$2p_7$	$2p_8$	$2p_9$	$2p_{10}$
$3s_2$	0.5 ±0.1 7305	(1.0)[T] (6401)[C]	0.79 ±0.17 6352	(1.9)[T] (6328)[C]	1.3 ±0.3 6294	0.81 ±0.15 6118	0.47 ±0.09 6046	0.38 ±0.07 5939	___	0.42 ±0.07 5434
$3s_3$	___	0.28 ±0.06 6422	___	___	1.8 ±0.4 6314	___	0.26 ±0.06 6065	___	___	<0.1 5449
$3s_4$	0.98 ±0.23 7725	(0.12)[T] 6721	1.1 ±0.5 6667	(0.28)[T] ( )[ℓ]	(2.7)[T] 6603	3.2 ±0.5 6410	(3.0)[T] (6331)[C]	7.4 ±2.0 (6214)[C]	___	1.0 ±0.2 5663
$3s_5$	___	0.12 ± .04 6760	___	(0.66)[T] (6678)[C]	<0.1 6640	0.65 ±0.15 6445	0.16 ±0.04 6365	0.58 ±0.12 (6247)[C]	2.5 ±0.4 (6182)[C]	0.81 ±0.07 5690
$\sum_{3s} Q_{jk}$	1.5 ±0.3	1.5 ±0.3	1.9 ±0.7	2.8 ±0.6	5.8 ±1.2	4.7 ±0.8	3.9 ±0.8	8.4 ±2.2	2.5 ±0.4	2.2 ±0.3

TABLE 6. Absolute Cross Sections of the Spectral Lines for the Series $4s \rightarrow 2p$

The upper number in each entry is the value of Q_{jk} at 100 eV in units of 10^{-20} cm^2 and the lower number is the corresponding wavelength in Å.

	$2p_1$	$2p_2$	$2p_3$	$2p_4$	$2p_5$	$2p_6$	$2p_7$	$2p_8$	$2p_9$	$2p_{10}$
$4s_2$	$(0.13)^T$	0.39 ±0.07	0.14 ±0.02	1.1 ±0.2	0.22 ±0.04	0.25 ±0.04	<0.1	0.12 ±0.02	—	0.18 ±0.02
	$(5967)^C$	5349	5315	5298	5274	5150	5099	5023		4656
$4s_3$	—	$<(0.1)^T$	—	—	0.10 ±0.01	—	<0.1	—	—	<0.1
		$(5355)^C$			5280		5105			4661
$4s_4$	$(0.15)^T$	<0.1	0.20 ±0.03	$<(0.1)^T$	0.33 ±0.06	0.94 ±0.14	0.79 ±0.09	1.6 ±0.4	—	0.28 ±0.05
	$(6250)^C$	5576	5539	$(\ )^{\ell}$	5494	5360	5305	5222		4827
$4s_5$	—	<0.1	—	<0.1	<0.1	0.22 ±0.04	<0.1	0.12 ±0.02	0.61 ±0.08	0.17 ±0.03
		5589		5534	5507	5372	5317	5234	5189	4837
$\sum_{4s} Q_{jk}$	$(0.28)^T$	0.39 ±0.07	0.34 ±0.05	1.1 ±0.2	0.65 ±0.11	1.4 ±0.2	0.79 ±0.09	1.8 ±0.4	0.61 ±0.08	0.63 ±0.10

TABLE 7. Absolute Cross Sections of the Spectral Lines

for the Series $\sum_{5,6,7,8,9}$ $ns \rightarrow 2p$

Each entry is the value of $\sum_{n} Q_{jk}$ at 100 eV in units of 10^{-20} cm^2.

	$2p_1$	$2p_2$	$2p_3$	$2p_4$	$2p_5$	$2p_6$	$2p_7$	$2p_8$	$2p_9$	$2p_{10}$
ns_2	<0.1	0.12 ±0.02	<0.1	0.7 ±0.1	0.10 ±0.01	0.14 ±0.04	<0.1	<0.1	—	<0.1
ns_3	—	<0.1	—	—	<0.1	—	<0.1	—	—	<0.1
ns_4	0.10 ±0.02	<0.1	0.11 ±0.01	<0.1	0.14 ±0.03	0.48 ±0.05	0.44 ±0.12	0.84 ±0.17	—	0.13 ±0.03
ns_5	—	<0.1	—	<0.1	<0.1	0.10 ±0.01	<0.1	<0.1	0.28 ±0.05	<0.1
$\sum_{ns} Q_{jk}$	0.10 ±0.02	0.12 ±0.02	0.11 ±0.01	0.7 ±0.1	0.24 ±0.04	0.72 ±0.10	0.44 ±0.12	0.84 ±0.17	0.28 ±0.05	0.13 ±0.03

transition probabilities, although they do not experience transitions to the ground state.

Since theory dominates the results of Table 8 and because of Fajen's discovery, one must conclude that these numbers can serve only to indicate relative magnitudes and, hence, no quantitative significance should be attached to them.

Finally, it should be mentioned that since this work represents the first known attempt to determine the apparent excitation cross sections of the ns families, comparison with other investigators is impossible.

TABLE 8. Estimation of Apparent Excitation Cross Sections of the ns Families

Upper Level	$\sum_k Q_{jk}$ at 100 eV in units of 10^{-20} cm^2	Percent Affected by Theory
$2s_3$	<3.9	62
$3s_3$	5.7	60
$4s_3$	0.3	70
$2s_5$	14	81
$3s_5$	10	52
$4s_5$	2.8	61
$2s_2$	110	90
$3s_2$	44	90
$4s_2$	14	83
$2s_4$	110	78
$3s_4$	106	87
$4s_4$	29	86

CHAPTER VI

CASCADE ANALYSIS OF THE 2p AND 2s FAMILIES

Under conditions of low electron beam current and atom number densities and when steady state conditions exist, the decrease in the population of an excited level due to radiative transitions will be equal to its gain in population due to cascading transitions from levels of higher energy and by direct excitation produced as a result of electron bombardment of ground state atoms. Since this investigation was carried out under these conditions, at least in most instances, the direct excitation cross section of an arbitrary jth excited level can be obtained directly by merely subtracting from the apparent excitation cross section all contributions due to cascade (refer back to equation 8). Beam currents and gas pressures were increased occasionally in order to obtain sufficient intensity from some of the weaker transitions so that an upper limit could be placed upon the value of their cross section.

In this investigation the effects of cascade upon the direct excitation cross section have been considered in a number of cases. This chapter presents the results of some of these considerations. Tabulated here for convenience are the estimates that were necessarily made in order to obtain the direct excitation cross sections of the ten 2p neon levels. Also given are the results of a similar determination of the cascade contribution from only the 3p family into the 2s family.

All results presented are for an electron energy of 100 eV.

The 2p Family

Tables 4-7 of the previous chapter and Tables 9-11 of this chapter list the necessary information to allow a complete cascade analysis of all ten 2p levels. For future reference the wavelengths of those spectral lines contributing significantly to the cascade into the 2p levels have been tabulated. Theoretical transition probabilities were used rather extensively in determining most of the entries in Tables 4 and 9-a for the following reasons:

(1) Most of the lines associated with the 2s family and some of the lines connecting the 3d→ 2p levels are beyond the spectral range of any presently existing photomultiplier tube.

(2) Due to low radiation intensity from many of the spectral lines, adequate signal could not be obtained from the photomultiplier tube without increasing the slit width of the monochromator. This procedure resulted in the loss of adequate resolution of a few desired spectral lines.

Thus, the Q_{jk} values entered in Tables 4 and 9-a, acquired by employing transition probabilities, were so obtained because of either or both of these two reasons.

It should be noted that transition probabilities were also used in Tables 5, 6, and 10. The reason for this was not because the spectral range to which the lines associated with the 3s, 4s, and 4d levels belong could not be reached by photomultiplier tubes, but was due to at least two factors:

(1) Some of the lines have never been reported in the literature. The

TABLE 9-a. Absolute Cross Sections of the Spectral Lines for the Series 3d→ 2p

Each entry is the value of Q_{jk} at 100 eV in units of 10^{-20} cm^2.

	$2p_1$	$2p_2$	$2p_3$	$2p_4$	$2p_5$	$2p_6$	$2p_7$	$2p_8$	$2p_9$	$2p_{10}$
$3s'_1$	2.5 ±0.5	4.4 ±0.9	$(5.0)^T$	$(0.14)^T$	$(0.58)^T$	$(0.20)^T$	2.0 ±0.4	$(0.18)^T$	—	1.2 ±0.1
$3s''_1$	—		—	$<(0.1)^T$	$<(0.1)^T$	$(0.17)^T$		$<(0.1)^T$	$\sim(0)^T$	0.46 ±0.07
$3s'''_1$	—	—	—	3.7 ±0.7	—	$(1.1)^T$	—	0.7±0.3	$<(0.1)^T$	—
$3s''''_1$	—	$\sim(0)^T$	—		1.2 ±0.2	$<(0.1)^T$	$(1.3)^T$	$<(0.1)^T$	$<(0.1)^T$	$\sim(0)^T$
$3d'_1$	—	—	—	$(0.81)^T$	—	$(2.2)^T$	—	0.86 ±0.17	1.5 ±0.3	—
$3d''_1$	—	$\sim(0)^T$	—	$<(0.1)^T$	0.39 ±0.08	$<(0.1)^T$	$(0.57)^T$			$\sim(0)^T$
$3d_2$	$(4.7)^T$	$<(0.1)^T$	$(4.6)^T$	1.5 ±0.3	5.1 ±1.1	$<(0.1)^T$	$(7.8)^T$	2.2 ±0.4	—	2.9 ±0.3
$3d_3$	—	$<(0.1)^T$	—	4.3 ±0.8	$<(0.1)^T$	2.2 ±0.6	$<(0.1)^T$	$<(0.1)^T$	$(0.15)^T$	1.8 ±0.2
$3d_4$	—	—	—		—	$(0.91)^T$	—	4.2 ±0.8	3.4 ±0.7	—
$3d'_4$	—	—	—	—	—	—	—	—		—

TABLE 9-a. (Continued)

	$2p_1$	$2p_2$	$2p_3$	$2p_4$	$2p_5$	$2p_6$	$2p_7$	$2p_8$	$2p_9$	$2p_{10}$
$3d_5$	$(0.31)^T$	1.3 ±0.3	1.1 ±0.2	$(0.65)^T$	$\sim(0)^T$	1.3 ±0.2	$<(0.1)^T$	$(0.27)^T$	—	7.9 ±0.6
$3d_6$	—		—	—	$<(0.1)^T$	—	$<(0.1)^T$	—	—	1.0 ±0.3
$\sum_{3d} Q_{jk}$	7.5 ±1.5	5.7 ±1.2	11±2	11±2	7.3 ±1.5	8.1 ±1.6	12±2	8.4 ±1.7	5.1 ±1.0	15±2

TABLE 9-b. Wavelengths of the Spectral Lines for the Series $3d \rightarrow 2p$

All numbers given are in Å.

	$2p_1$	$2p_2$	$2p_3$	$2p_4$	$2p_5$	$2p_6$	$2p_7$	$2p_8$	$2p_9$	$2p_{10}$
$3s'_1$	10,562	8,772	8,680	8,635	8,571	8,249	8,119	7,927	—	7,051
$3s''_1$	—	8,784	—	8,647	8,583	8,259	8,129	7,937	7,833	7,059
$3s'''_1$	—	—	—	8,654	—	8,266	—	7,943	7,839	—
$3s''''_1$	—	8,793	—	8,656	8,591	8,267	8,136	7,944	( )[l]	7,065
$3d'_1$	—	—	—	9,220	—	8,781	—	8,417	8,302	—
$3d''_1$	—	9,377	—	9,222	9,149	8,782	8,635	8,418	8,300	( )[l]
$3d_2$	11,536	9,433	9,327	9,276	9,222	8,831	8,682	8,463	—	7,472
$3d_3$	—	9,459	—	9,301	9,227	8,854	8,704	8,485	8,366	7,489
$3d_4$	—	—	—	9,314	—	8,866	—	8,495	8,376	—
$3d'_4$	—	—	—	—	—	—	—	—	8,378	—
$3d_5$	11,688	9,534	9,425	9,373	( )[l]	8,919	8,768	8,545	—	7,536
$3d_6$	—	9,547	—	—	9,311	—	8,779	—	—	7,544

TABLE 10. Absolute Cross Sections of the Spectral Lines for the Series 4d→ 2p

The upper number in each entry is the value of Q_{jk} at 100 eV in units of 10^{-20} cm^2 and the lower number is the corresponding wavelength in Å.

	$2p_1$	$2p_2$	$2p_3$	$2p_4$	$2p_5$	$2p_6$	$2p_7$	$2p_8$	$2p_9$	$2p_{10}$
$4s'_1$	0.73 ±0.15	1.5 ±0.3	2.2 ±0.3	<0.1	0.40 ±0.05	<0.1	0.40 ±0.06	<0.1	—	0.40 ±0.04
	6738	5962	5919	5898	5868	5715	5653	5559		5114
$4s''_1$,$4s'''_1$, $4s''''_1$	—	0.75 ±0.08	—	1.7 ±0.3	0.60 ±0.06	0.13 ±0.02	0.20 ±0.02	0.22 ±0.02	~(0)[T]	0.20 ±0.02
		5965		5902	5873	5719	5657	5563	5511	5116
$4d'_1$	—	~(0)[T]	—	0.15 ±0.03	(0.41)[T]	(0.40)[T]	0.54 ±0.05	0.35 ±0.04	0.34 ±0.04	~(0)[T]
$4d''_1$		( )[ℓ]		6175	6143	5975	5906	5804	5748	5321
$4d_2$	0.80 ±0.10	<0.1	2.1 ±0.2	(0.30)[T]	2.0 ±0.2	1.1 ±0.6	3.3 ±0.5	0.88 ±0.13	—	0.41 ±0.07
	7112	6253	6206	6183	6150	5982	5914	5811		5326
$4d_3$	—	<0.1	—	0.20 ±0.05	<0.1	0.33 ±0.05	<0.1	<0.1	<0.1	0.48 ±0.05
		6259		6189	6156	5988	5919	5817	5761	5331

TABLE IO. (Continued)

	$2p_1$	$2p_2$	$2p_3$	$2p_4$	$2p_5$	$2p_6$	$2p_7$	$2p_8$	$2p_9$	$2p_{10}$
$4d_4$	—	—	—	<0.1	—	0.35 ±0.04	—	1.6 ±0.2	1.1 ±0.2	—
$4d'_4$				6193		5992		5820	5764	
$4d_5$	$(0.20)^T$	$(0.75)^T$	$(0.34)^T$	$(0.39)^T$	<0.1	0.5 ±0.1	<0.1	0.20 ±0.05	—	2.2 ±0.2
$4d_6$	$(\ )^{\ell}$	6273	6226	6203	6173	6001	5934	5829		5341
$\sum_{4d} Q_{jk}$	1.7 ±0.3	3.0 ±0.6	4.6 ±0.9	2.7 ±0.5	3.4 ±0.7	2.8 ±0.8	4.4 ±0.6	3.3 ±0.4	1.4 ±0.2	3.7 ±0.4

TABLE 11. Absolute Cross Sections of the Spectral Lines for the Series $\sum_{5,6,7}$ nd→ 2p

Each entry is the value of $\sum_{u} Q_{jk}$ at 100 eV in units of 10^{-20} cm^2, where u represents all the indicated upper states.

	$2p_1$	$2p_2$	$2p_3$	$2p_4$	$2p_5$	$2p_6$	$2p_7$	$2p_8$	$2p_9$	$2p_{10}$
$ns'_1, ns''_1,$ ns'''_1, ns''''_1	0.38 ±0.08	0.72 ±0.14	0.5 ±0.1	0.93 ±0.18	0.32 ±0.06	0.16 ±0.03	0.30 ±0.06	0.14 ±0.03	<0.1	0.52 ±0.10
$nd'_1, nd''_1,$ nd_2, nd_3 $nd_4, nd'_4,$ nd_5, nd_6	0.18 ±0.04	0.16 ±0.03	0.65 ±0.13	0.12 ±0.02	0.45 ±0.09	1.4 ±0.3	1.4 ±0.3	1.7 ±0.3	0.78 ±0.08	1.1 ±0.2
$\sum_{nd} Q_{jk}$	0.56 ±0.12	0.88 ±0.17	1.2 ±0.2	1.1 ±0.2	0.77 ±0.15	1.6 ±0.3	1.7 ±0.4	1.8 ±0.3	0.78 ±0.08	1.6 ±0.3

space which would be occupied by their wavelengths, if they existed, have been noted by the entries ( )$^{\ell}$.

(2) Some of the spectral lines reported in these three tables were just too close to neighboring lines of greater intensity to be satisfactorily separated from the more intense ones by the monochromator. Therefore, the only way to determine the cascade contribution from these transitions was to first find spectral lines originating from the same upper level that could be isolated and detected, measure their cross sections, and then from these values make the appropriate estimates by employing transition probabilities.

It is, of course, understood that an analysis of this type would yield much more satisfactory results if one did not have to rely so heavily on theory, for after all the ultimate reason for performing the experiment was to obtain a check on the theory and it does seem a little strange to use theory to test theory. Nevertheless, since a purely experimental solution to the 2p cascade problem could not be obtained, this approach was necessary. As it turns out, the cascade estimates obtained by theory are such a small fraction of the total contribution to any given 2p level anyway that the final results should yield a significant test of the theory.

For those transitions where theoretical transition probabilities are used to determine the Q_{jk} value, it is impossible to place limits of error upon the number entered in the table. The purely experimental measurements generally varied from one determination to the next for individual transitions to within 20 per cent. A few cases where this error is larger are reported for some of the weaker transitions.

Tables 7 and 11 were obtained strictly by experiment. Since many

of the levels merge as the n value is increased, especially the nd families, resolution of the spectral lines presented a real problem. As one goes to higher n values the ns_1', ns_1'', ns_1''', and ns_1'''' levels shift closer to each other while at the same time the nd_1', nd_1'', ..., nd_6 levels also shift closer to each other. Thus, the radiation into the 2p levels coming from the d levels is reported in Table 11 for n values of 5, 6, and 7 as though it originated from two distinct levels, i.e. those designated in the Paschen notation by placing primes on the letter s and those symbolized by the true letter d. The merging of levels for increasing n values can also exist for the ns families, i.e. ns_2 and ns_3 merge while at the same time ns_4 and ns_5 merge. In Table 7, however, the identity of the upper level has been retained.

The cross sections of those transitions originating at levels greater than 9s or 7d were found to be less than 10^{-22} cm^2 at 100 eV. This represents the detectivity limit of the system employed in this investigation. Inasmuch as all lines reported in the tables with cross sections less than 10^{-21} cm^2 were neglected in the total cascade contribution, further neglect of these lines certainly introduces a negligible error in the final result.

Adding the individual Q_{jk} entries in each column of Tables 4-7 and 9-11 will yield the total cascade contribution into the separate 2p neon levels. These sums have been obtained and the results are presented in the form of percentages in Table 12. Also included in this same table are the resulting experimental direct excitation cross sections along with those calculated by Fred E. Fajen[2] using the Born-Ochkur approximation.

An examination of this table reveals discrepancies between experiment

TABLE 12. Comparison Between Experiment and Theory At 100 eV for the Direct Excitation Cross Sections of the 2p Family

All cross sections are expressed in units of 10^{-20} cm^2.

Level	Direct Electron Excitation		Percent of Cascade
	Theory	Experiment*	
$2p_1$	690	160	8
$2p_2$	0.22	23	45
$2p_3$	14	15	59
$2p_4$	9.60	64	33
$2p_5$	7.10	17	59
$2p_6$	37	62	36
$2p_7$	1.50	23	58
$2p_8$	7.60	40	54
$2p_9$	3.90	18	50
$2p_{10}$	14	17	67

*A maximum error of 20 percent is placed upon the experimental values. Uncertainties introduced due to theoretical transition probabilities employed in this analysis are unknown to this author. Therefore, the 20 percent figure merely represents an estimate of the actual error which could possibly exist from this analysis.

and theory with the theoretical to experimental ratio ranging from a factor .01 to 4.3. Due to the large variations in some cases, it is perhaps quite accidental that such nearly perfect agreement does exist between theory and experiment for the $2p_3$ and $2p_{10}$ levels. It is interesting to note that all theoretical results, with the exception of the $2p_1$ cases, are smaller than those for the corresponding experimental values. The largest discrepancy between theory and

experiment occurs for the $2p_2$ level. Since the theoretical value is quite small for this level, it is not too surprising that such a large difference does exist between the two approaches, for theory can yield a rather absurd result when the final answer is small. This is because in any type of approximation, which must be used to calculate theoretical excitation cross sections, it is possible to neglect a small number which could affect the final result quite significantly. Judging from previous conclusions which have been drawn between theory and experiment for other gases, it is felt that a factor of five between the two approaches to the neon problem is not too surprising. While the overall agreement is not poor, the above results do suggest that more accurate theoretical calculations are needed.

For the benefit of completeness and to facilitate future determination of the direct excitation cross section of any desired 2p level for a different energy other than 100 eV, representative excitation functions of the d levels are included in this paper.

Since the d levels are spaced so closely to each other, it was experimentally impossible to obtain excitation functions to represent exclusively the apparent cross sections of the 12 individual nd levels. For example, the excitation function of any nd_4' level could not be obtained devoid of nd_4 radiation. Also nd_1'' radiation contaminated the excitation functions of the nd_1' levels or vice versa. Similar statements can be made regarding ns_1'', ns_1''', and ns_1''''. The only d levels which yield excitation functions free of contaminating radiation from other levels are the ns_1', nd_2, nd_3, nd_4, nd_5, and nd_6 levels. For those levels where the associated spectral lines connecting the 2p family could not be sufficiently resolved to yield excitation functions free of

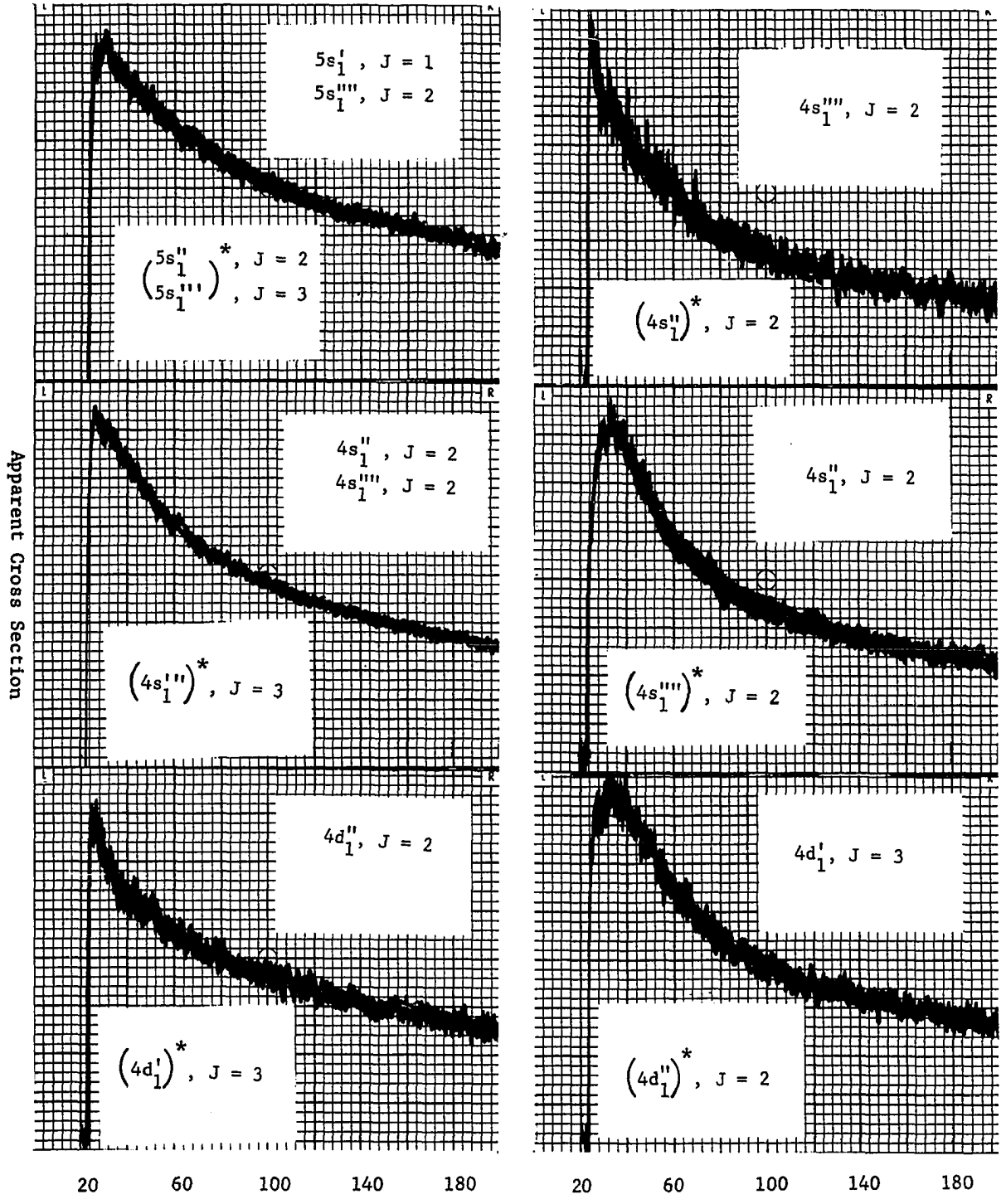

FIGURE 16a. Representative Excitation Functions of the d Levels

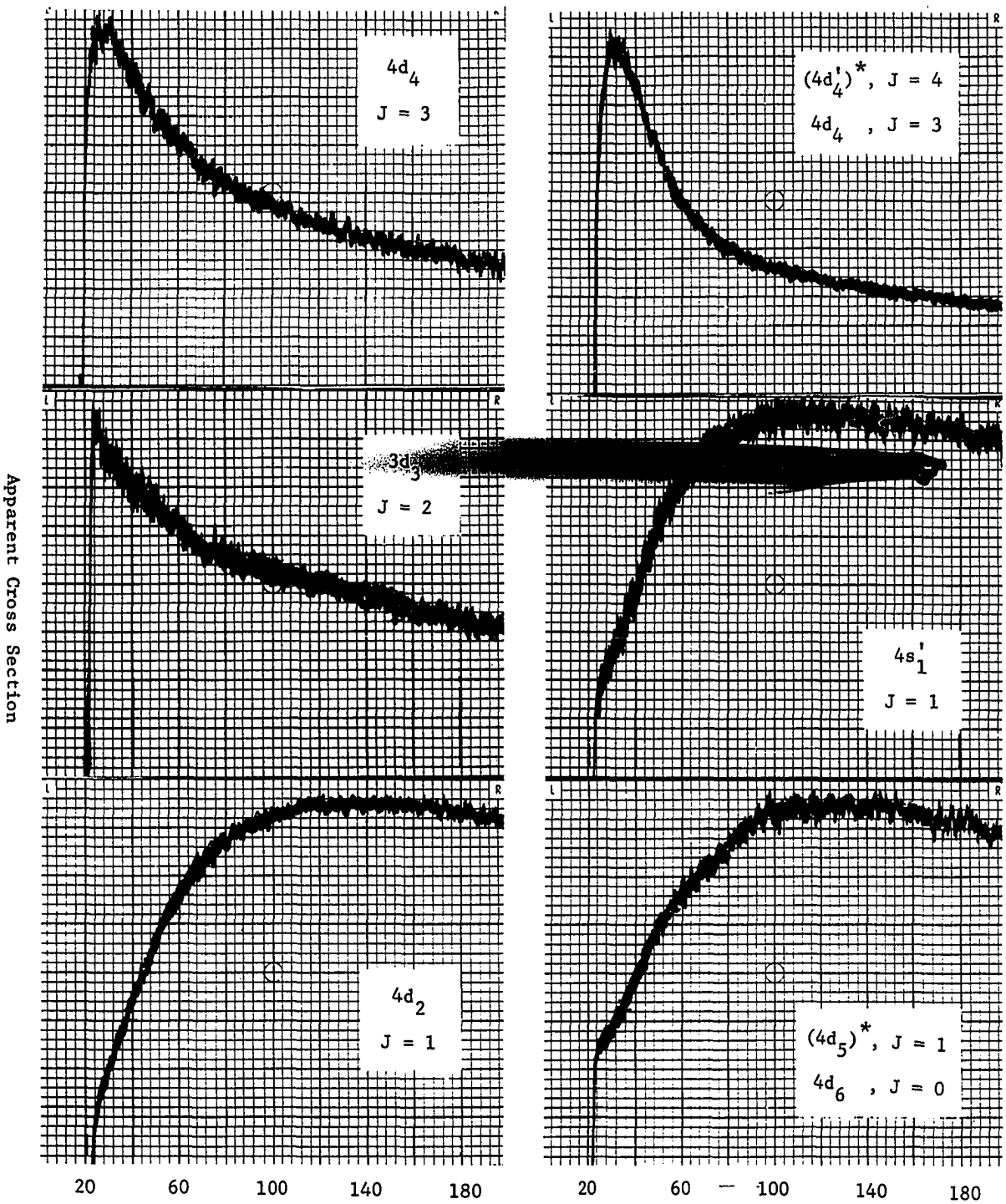

FIGURE 16b. Representative Excitation Functions of the d Levels

contaminating radiation, curves are presented which primarily represent the excitation functions of the desired upper levels. These curves were obtained from spectral lines whose radiation was known to be predominately from that of the upper level whose excitation function was desired. The curves so obtained and presented in Figures 16a and 16b have those upper levels, marked by an asterisk (*), which are known to contribute the largest percentage of the radiation. The excitation function of the $3d_6$ level, closely resembling that of the $3d_3$ level, was obtained but the resulting curve contained so much detector noise that it was felt the data would not be useful. Since the nd_6 levels do not contribute significantly to the cascade (the major transition being $3d_6 \rightarrow 2p_{10}$), the exclusion of the curve, or even the $nd_6 \rightarrow 2p$ transition altogether for that matter, would not introduce a noticeable error into the final result. Furthermore, values of $n \geq 4$ resolution of the spectral lines originating at all nd_6 levels could not be resolved from those originating at the corresponding nd_5 levels. Therefore, the results may be considered as the total contribution from both levels and the $(4d_5)^*$, $4d_6$ curve given in Figure 16b used to obtain the cross section, i.e. at least for the $np_6 \rightarrow 2p_{10}$ cases which are the only ones necessary to consider.

A few points of interest may be noted from the curves presented in Figures 16a and 16b. Most of the excitation functions have sharp peaks and tails that decline with varying degrees of rapidity for increasing energy. The only excitation functions with very broad, almost flat, peaks are those of the levels which have allowed optical transitions to the ground state, i.e. the ns'_1, nd_2, and nd_5 levels. The argument given in the previous chapter for the s states pertaining

to the singlet and triplet mixing of the levels also applies to the d levels, but in this case, at least for most of the excitation functions, the triplet form seems to dominate the curves. The only pure triplet state of the d families is that corresponding to the nd'_4 levels.

The 2s Family

In order to determine what fraction of the apparent cross section of the s levels is produced by cascade, the contribution influencing the 2s family from radiation out of the 3p family was obtained. The 2s family was chosen since they would be the most affected by cascade of the s levels, and the 3p family would yield the major contribution. The results presented in Table 13 were obtained from the Q_{jk} values listed in Table 3 for the 3p→ 1s series. Transition probabilities listed in the Appendix were employed by the method given there in order to obtain the desired 3p→ 2s Q_{jk} values.

In the previous chapter it was stated that the shapes of the excitation functions implied that the cascade contribution into any s

TABLE 13. Cascade Contribution From 3p Into 2s Levels

Lower Level	$\sum_{3p} Q_{3p,2s}$ at 100 eV in Units of 10^{-20} cm^2	Percent of Cascade
$2s_2$	50	45
$2s_3$	2.8	> 72
$2s_4$	24	22
$2s_5$	12	86

level does not exceed about 20 percent. Although the percentages given here all exceed this margin, they are, however, not too surprising. It must be remembered that theoretical transition probabilities affect each entry. By slightly varying the wave functions of the 3p states, Fajen* has shown that the transition probabilities associated with the $3p \rightarrow 2s$ series are not affected, but those associated with the $3p \rightarrow 1s$ series can change by a factor of 15. Thus, it appears that a more agreeable result between experiment and theory can only be obtained when more accurate values of transition probabilities become available. The method, however, is sound and may be used later when accurate theoretical data becomes available.

*Private communication.

CHAPTER VII

SUMMARY

Excitation functions for 44 spectral lines of neon were obtained under conditions of low electron beam and ground state number densities. These curves illustrate the variation of the apparent cross sections of the s, p, and d levels over an energy range from onset to 200 eV. Similarities in the shapes of these curves and those obtained for the excited states of helium have been noted. The pure triplet states have been found to possess excitation functions which have sharp peaks and fast declining tails at higher energy. Those levels having optically allowed transitions to the ground state were discovered to have excitation functions characterized by very broad flat maximums quite similar to those of the ^1P states of helium.

Other similarities to helium include the following: the apparent cross sections of the pure triplet states are, in general, much smaller than those of the singlet states, and the cascade contribution into the s levels was observed qualitatively to be quite small.

Absolute measurements of the cross sections of over 250 spectral lines have yielded the experimental basis for the neon study. Extreme care was exercised in the measurements and several determinations were made so that the lack of repeatability in the experimental results could

be used to estimate the experimental errors.

Where possible, comparisons have been made with earlier experimental results but the methods employed in these few instances by those workers were so primitive that conclusive comments cannot be justifiably made.

The cross sections of the spectral lines associated with the 2p family were used to determine the direct excitation cross sections at 100 eV of all ten 2p levels. For those Q_{jk} values which could not be determined experimentally, theoretical transition probabilities or branching ratios were used to obtain the desired result. These were used only in determining cascade contributions into the 2p family. The total contribution obtained in this manner represents a small fraction of the total estimate. Thus, the results given in this work were primarily determined through experiment and the errors incurred should be largely due to the experimental method.

The direct excitation cross sections obtained by experiment have been compared with corresponding values resulting from theoretical calculations using the Born-Ochkur approximation. Although the agreement is not poor, it is quite evident that better theoretical calculations are needed.

A similar analysis was carried out in order to determine the cascade contribution into the four 2s levels from those belonging to the 3p family. In this case, however, the final result was completely affected by theory. The result implies that the cascade contribution is much larger than had been qualitatively predicted through examination of the excitation functions. It was found that a slight variation in the form of the wave functions describing the 3p states could affect

the transition probabilities which were used in the calculation by as much as a factor of 15. This discovery leaves the results of this latter analysis and, for that matter, any result obtained in this work which was largely affected by theory to be highly questionable.

This example illustrates one of the many difficulties of using the optical method to determine the direct excitation cross sections of the heavier atoms. In obtaining the excitation cross sections of all spectral lines involved in such a determination, one is forced to use theoretical transition probabilities. This requires accurate wave functions of the excited states and these are not generally available. This difficulty is not as severe in helium, but is reported by Anderson et al[1] to be quite serious in the case of mercury.

Thus, this author concludes that more accurate theoretical work needs to be done in conjunction with the experiment in order to make the optical method a more effective tool to study basic atomic and molecular excitation processes.

APPENDIX

LIST OF TRANSITION PROBABILITIES

The numbers given in this appendix were supplied by Fred E. Fajen[2] in order to carry out the cascade analysis presented in Chapter 6. Although the numbers are equivalent to transition probabilities in this application, technically they represent the product gA, where $g = (2J+1)$ is the statistical weight of the upper level and A is the spontaneous Einstein transition probability in units of sec^{-1}. The J value of all upper neon levels is given in the figures where their excitation functions are displayed. Hence, these numbers may be readily converted into transition probabilities; however, they were not needed to carry out the calculations which led to the results presented in Chapters 5 and 6. The basic quantity desired in this work was the Q_{jk} value of a particular $j \rightarrow k$ spectral transition after the $Q_{jk'}$ value of the $j \rightarrow k'$ transition was obtained from experimental measurement. In terms of $Q_{jk'}$ and the ratio of the respective transition probabilities involved, the Q_{jk} value may be obtained from the expression

$$Q_{jk} = \frac{A_{jk}}{A_{jk'}} Q_{jk'} \quad ,$$

where j represents the upper level and k, k' the two lower ones. Thus, the factor g is eliminated in the calculations and need not be determined.

gA in units of 10^7 sec^{-1}

	$2p_1$	$2p_2$	$2p_3$	$2p_4$	$2p_5$	$2p_6$	$2p_7$	$2p_8$	$2p_9$	$2p_{10}$	Ground State
$2s_2$	0.29	1.49	0.29	2.50	0.85	2.64	0.288	0.24	—	0.61	20.8
$2s_3$	—	0.66	—	—	0.85	—	1.30	—	—	0.50	—
$2s_4$	0.09	0.0023	0.51	0.27	0.755	1.20	1.40	3.58	—	1.00	16.0
$2s_5$	—	0.39	—	1.44	0.20	1.21	0.204	1.51	7.47	3.13	—
$3s_2$	0.091	0.382	0.11	0.699	0.15	0.484	0.121	0.139	—	0.162	5.99
$3s_3$	—	0.182	—	—	0.226	—	0.314	—	—	0.095	—
$3s_4$	0.061	0.012	0.119	0.028	0.273	0.441	0.313	0.804	—	0.158	8.29
$3s_5$	—	0.124	—	0.442	0.060	0.337	0.055	0.39	1.88	0.653	—
$4s_2$	0.040	0.166	0.054	0.314	0.058	0.191	0.061	0.075	—	0.073	2.60
$4s_3$	—	0.081	—	—	0.100	—	0.136	—	—	0.039	—
$4s_4$	0.033	0.0084	0.050	0.0079	0.130	0.213	0.130	0.338	—	0.061	4.33
$4s_5$	—	0.057	—	0.202	0.027	0.151	0.025	0.172	0.824	0.276	—
$3s_1'$	1.92	3.55	5.13	0.145	0.60	0.209	2.01	0.19	—	1.24	10.8
$3s_1''$	—	17.40	—	1.35	0.124	2.33	0.481	0.885	0.033	6.43	—
$3s_1'''$	—	—	—	23.60	—	9.75	—	5.98	0.104	—	—
$3s_1''''$	—	0.002	—	1.79	12.50	0.936	13.50	0.171	0.005	0.00	—

	$2p_1$	$2p_2$	$2p_3$	$2p_4$	$2p_5$	$2p_6$	$2p_7$	$2p_8$	$2p_9$	$2p_{10}$	Ground State
$3d_1'$	—	—	—	6.32	—	17.20	—	0.905	11.70	—	—
$3d_1''$	—	0.00	—	0.92	6.31	0.033	9.22	8.66	0.586	0.00	—
$3d_2$	1.72	0.032	1.70	0.39	3.74	0.028	2.84	1.01	—	1.06	22.1
$3d_3$	—	0.816	—	4.79	0.707	5.77	0.493	0.429	1.33	15.60	—
$3d_4$	—	—	—	0.375	—	6.34	—	29.20	2.05	—	—
$3d_4'$	—	—	—	—	—	—	—	—	52.10	—	—
$3d_5$	0.48	1.66	1.12	0.999	0.0009	1.12	0.013	0.409	—	12.1	7.03
$3d_6$	—	0.787	—	—	0.387	—	0.376	—	—	5.01	—
$4s_1'$	0.485	0.625	0.875	0.037	0.155	0.031	0.286	0.02	—	0.246	7.78
$4s_1''$	—	3.08	—	0.319	0.050	0.285	0.094	0.125	0.001	1.27	—
$4s_1'''$	—	—	—	4.06	—	1.98	—	1.07	0.0027	—	—
$4s_1''''$	—	0.0045	—	0.319	2.08	0.173	2.54	0.062	0.0001	0.0019	—
$4d_1'$	—	—	—	1.45	—	2.96	—	0.116	2.06	—	—
$4d_1''$	—	0.00	—	0.201	1.38	0.01	1.49	1.51	0.103	0.00	—
$4d_2$	0.394	0.010	0.440	0.059	0.690	0.0037	0.580	0.179	—	0.098	13.0
$4d_3$	—	0.293	—	0.871	0.128	1.18	0.102	0.096	0.243	2.26	—

	$2p_1$	$2p_2$	$2p_3$	$2p_4$	$2p_5$	$2p_6$	$2p_7$	$2p_8$	$2p_9$	$2p_{10}$	Ground State
$4d_4$	—	—	—	0.079	—	1.18	—	5.29	0.373	—	—
$4d'_4$	—	—	—	—	—	—	—	—	9.32	—	—
$4d_5$	0.111	0.365	0.181	0.209	0.0004	0.22	0.00	0.089	—	2.00	3.86
$4d_6$	—	0.161	—	—	0.077	—	0.071	—	—	0.821	—

	$3p_1$	$3p_2$	$3p_3$	$3p_4$	$3p_5$	$3p_6$	$3p_7$	$3p_8$	$3p_9$	$3p_{10}$
$1s_2$	0.218	0.297	0.0099	0.687	0.184	0.179	0.148	0.178	—	0.0029
$1s_3$	—	0.222	—	—	0.466	—	0.0119	—	—	0.0167
$1s_4$	0.0127	0.125	0.230	0.428	0.0449	0.180	0.399	0.576	—	0.133
$1s_5$	—	0.0513	—	0.0228	0.0035	0.810	0.118	0.379	1.67	0.531
$2s_2$	0.789	1.06	0.0245	2.69	0.567	0.0716	0.0127	0.0074	—	0.0110
$2s_3$	—	0.581	—	—	1.19	—	0.0199	—	—	0.0189
$2s_4$	0.0701	0.0126	0.719	0.140	0.0006	0.865	1.41	1.82	—	0.226
$2s_5$	—	0.204	—	0.0908	0.0134	2.26	0.325	0.977	4.12	1.08

	$3p_1$	$3p_2$	$3p_3$	$3p_4$	$3p_5$	$3p_6$	$3p_7$	$3p_8$	$3p_9$	$3p_{10}$
$3s_2$	0.0895	0.375	0.0370	0.979	0.212	0.0297	0.0003	0.0050	—	0.0627
$3s_3$	—	0.175	—	—	0.389	—	0.0193	—	—	0.0419
$3s_4$	0.0046	0.0006	0.106	0.0004	0.0027	0.294	0.467	0.726	—	0.154
$3s_5$	—	0.0146	—	0.0065	0.0011	0.563	0.0846	0.310	1.47	0.651
$4s_2$	0.0358	0.109	0.0116	0.287	0.0594	0.0041	0.0008	0.0032	—	0.0137
$4s_3$	—	0.0532	—	—	0.115	—	0.0043	—	—	0.0078
$4s_4$	0.0047	0.0008	0.0383	0.000	0.0019	0.0903	0.139	0.202	—	0.0346
$4s_5$	—	0.0075	—	0.0033	0.0005	0.182	0.0269	0.0927	0.424	0.162

	$4p_1$	$4p_2$	$4p_3$	$4p_4$	$4p_5$	$4p_6$	$4p_7$	$4p_8$	$4p_9$	$4p_{10}$
$4s_2$	0.0346	0.115	0.0056	0.296	0.0698	0.0029	0.000	0.0004	—	0.0096
$4s_3$	—	0.0646	—	—	0.112	—	0.0015	—	—	0.0062
$4s_4$	0.000	0.000	0.0311	0.000	0.000	0.0874	0.142	0.216	—	0.0410
$4s_5$	—	0.0002	—	0.000	0.000	0.172	0.0248	0.0903	0.431	0.191

LIST OF REFERENCES

1. Anderson, Richard J., Edward T. P. Lee and Chun C. Lin, Physical Review 157 (1967), p. 31.

2. Fajen, Fred E., Unpublished Data from the Los Alamos Scientific Laboratory.

3. Anderson, Richard J., Excitation of Mercury Atoms by Electron Impact, Dissertation, University of Oklahoma, 1966.

4. Harrison, George R., Richard C. Lord and John R. Loofbourow, Practical Spectroscopy. New York: Prentice-Hall, Inc., 1954, p. 137.

5. Devos, J. C., Physica 20 (1954), p. 715.

6. Racah, G., Physical Review 61 (1942), p. 537.

7. Paschen, F. and R. Gotze, Serien-gesetze Der Leniensplktren. Berlin: Verlag von Julius Springer, 1922, p. 20.

8. Paschen, F., Annalen der Physik 60 (1919), p. 405.

9. Paschen, F., Annalen der Physik 63 (1920), p. 201.

10. Jongerius, H. M., Measurements of Optical Excitation Functions of the Mercury Atom (Excitation by Electrons), Dissertation, University of Utrecht, 1961.

11. Schulz, G. J., Physical Review Letters 10 (1963), p. 104.

12. Schulz, G. J., Physical Review 116 (1959), p. 1141.

13. Schulz, G. J. and R. E. Fox, Physical Review 106 (1957), p. 1179.

14. Baranger, Elizabeth and Edward Gerjuoy, Physical Review 106 (1957), p. 1182.

15. Hanle, W., Zeitschrift für Physik 65 (1930), p. 512.

16. Herrmann, Oskar, Annalen der Physik 25 (1936), p. 143.

17. Milatz, J. M. W. and J. P. M. Woudenberg, Physica 7 (1940), p. 697.

18. Frish, S. E., Optics and Spectroscopy (U.S.S.R.) 15 (1963), p. 395.

19. Zapesochnyi, I. P. and P. V. Fel T San, Bulletin Academy of Science U.S.S.R., Physics Serial 27 (1963), p. 1015.

20. Irwin, J. C. and R. A. Nodwell, Canadian Journal of Physics 44 (1966), p. 1781.